

DEVELOPMENT OF KERATIN BASED ORGANO-APATITES AS BONE-MIMETIC BIOMATERIALS

A Thesis submitted in partial fulfillment of the requirements for the degree of

Master of Technology

In

Biotechnology

By

JOSEPH CHRISTAKIRAN M.

(Reg. No. 213BM2028)

Under the supervision of

Prof. Krishna Pramanik



Department of Biotechnology & Medical Engineering

National Institute of Technology, Rourkela

Rourkela-769008, Orissa, India

June, 2015



NATIONAL INSTITUTE OF TECHNOLOGY, ROURKELA

CERTIFICATE

This is to certify that the thesis entitled “**Development of Keratin based Organo-apatites as Bone-mimetic Biomaterials**” by **Joseph Christakiran M.** (Reg. No. **213BM2028**) submitted to the National Institute of Technology, Rourkela for the award of Master of Technology in Biotechnology during the session 2013-2015, is a record of bonafide research work carried out by him in the Department of Biotechnology and Medical Engineering under my supervision and guidance. To the best of my knowledge, the matter embodied in the thesis has not been submitted to any other University / Institute for the award of any Degree or Diploma.

Prof. Krishna Pramanik

Professor & Head

Department of Biotechnology & Medical Engineering

National Institute of Technology

Rourkela-769008

ACKNOWLEDGEMENTS

First of all I take great delight in thanking God Almighty, for His blessings and grace that enabled me to complete my project with great satisfaction. On a personal note, I express my deep sense of gratitude to my dear parents, Mr. and Mrs. Moses Sathyaveera for their untiring love and encouragement.

I express my heartfelt gratitude to my supervisor, Prof. Mrs. Krishna Pramanik for her valuable guidance and constant monitoring throughout the course of the project. I would like to record my indebtedness to Prof. Dr. Sirsendu Sekhar Ray for his constant moral support, valuable suggestions and for creating a friendly environment and enabling me to use the resources in the Anatomy and Physiology Lab, Department of Biotechnology and Medical Engineering, NIT-Rourkela.

I express my sincere gratitude to my teachers, Prof. Indranil Banerjee, Prof. B. P. Nayak, Prof. Mukesh Gupta, Prof. Subhankar Paul, Prof. A. Thirugnanam and Prof. Nandini Sarkar for their teaching expertise and support which helped mold me in my Post graduation programme.

I am ever grateful to Mr. Senthilguru Kulanthaivel (Research scholar, Biotechnology), Ms. Tejinder Kaur Sandhu (Research scholar, Biotechnology), Mr. Bheesham N. Singh (Research scholar, Biotechnology), Dr. Akalabya Bissoyi (Post-doctoral fellow, Biotechnology), Mr. Deependra Kumar Ban (Research scholar, Biotechnology) and Mr. Ezhil Venuswaran (Research scholar, Ceramic Engineering), from whom I learnt the essence of research practice and for motivating me throughout the course of my dissertation work. I would like to thank Mr. Arvind Kumar (Ceramic Engineering) and Mr. Sushanth Pradhan (Biotechnology and Medical Engineering) for their technical assistance in operating the instruments related to characterizations of my samples.

I feel my acknowledgements are incomplete unless and until I thank my dear friends, Gautham Hari Narayana S. N., Narendra Babu P., Anupriya Bharathirajan, Vinay Kumar, Rakesh Bhulan, Trupti Patil and Usha Pandey whose motivation, support and kindness they extended towards me during the entire tenure of my stay at NIT-Rourkela, was unforgettable and heart gladdening.

Joseph Christakiran M.

ABSTRACT

The bone is a hierarchically built organ by a bottom-up approach consisting of organo-apatite building blocks of mineralized collagen. In order to develop a bone-mimetic material, hard α -keratin a structural protein extracted from human hair was used as a template for the synthesis of keratin based organo-apatites in this study. A comparative study was done to analyze the stability of the keratin extracted by two different methods namely Shindai and sodium sulfide methods. It was found that the sodium sulfide method was relatively better for extraction of keratin because of its enhanced yield, ease of extraction, stability of the extracted protein and conservation of structural integrity of the extracted keratin. The keratin extracted by sodium sulfide method was used as a template for the synthesis of 5 different organo-apatites namely HAP-K50, HAP-K75, HAP-K100, HAP-K125 and HAP-K150 with different concentrations of keratin through co-precipitation method. The phase analysis of the synthesized keratin based organo-apatites was done using XRD which revealed the keratin in the composites decreased the crystallinity and size of the apatite formed. The functional analysis done using FTIR and CD and the morphological observation using FESEM showed heterogeneous nucleation and growth of 20-30nm apatite crystals along the keratin fibril. The thermal analysis helped to determine the ratio of organics and inorganics present in the composites. The composites HAP-K100 and HAP-K125 which had a ratio of organics to inorganics similar to that of the bone, showed higher bio-activity, superior cell viability and cell spreadability as compared to the other composites used under study. The enhanced osteogenic differentiation potential of these composites assessed through alizarin red assay, ALP assay and Runx2 and osteocalcin expression demonstrated that the composites HAP-K100 and HAP-K125 can be used as bone-mimetic biomaterials for bone tissue engineering applications.

Keywords: Keratin, sodium sulfide method, organo-apatites, bone-mimetic nano-composites, ADSCs, osteogenic differentiation

TABLE OF CONTENTS

ABSTRACT	i
LIST OF FIGURES	vi
LIST OF TABLES	ix
LIST OF ABBREVIATIONS	x
1. INTRODUCTION	
1.1 Background and significance of study	1
1.2 Architecture of the bone	2
1.3 Organo-apatites in bone tissue engineering	3
1.4 Keratin based organo-apatites	3
1.4.1 Keratin	4
1.4.2 Structure of hard-alpha keratin	4
1.4.3 Keratin as ideal polymer for organo-apatite synthesis	4
1.5 Objectives	5
2. LITERATURE REVIEW	
2.1 Extraction of keratin from human hair	6
2.1.1 Extraction of keratose	6
2.1.2 Extraction of keratiene	7
2.2 Effect of extraction procedure on protein folding	8
2.3 Synthesis of organo-apatites	9
2.4 Osteogenic differentiation of adult stem cells	12
2.5 Keratin and osteogenic differentiation potential	13
3. MATERIALS AND METHODS	
3.1 Materials	
3.1.1 Extraction of keratin	15
3.1.2 Synthesis of keratin based organo-apatites	15
3.1.3 Cell culture study	15
3.2 Methods	
3.2.1 Extraction of keratin from human hair	
3.2.1.1 Processing of human hair	15

3.2.1.2	Extraction protocols for human hair keratin	16
3.2.1.3	Protein quantification by Bradford's method	16
3.2.1.4	SDS-Polyacrylamide gel electrophoresis	17
3.2.1.5	Characterization of extracted keratin	
3.2.1.5.1	Fourier Transform Infrared Spectroscopy	17
3.2.1.5.2	Zeta potential and Dynamic Light Scattering	18
3.2.1.5.3	Circular Dichroism Spectroscopy	18
3.2.1.5.4	X-ray diffraction	18
3.2.2	Synthesis of keratin based organo-apatites	19
3.2.3	Characterization of organo-apatites	
3.2.3.1	X-ray diffraction	21
3.2.3.2	Field Emission Scanning Electron Microscopy	22
3.2.3.3	Functional analysis	
3.2.3.3.1	Fourier Transform Infrared Spectroscopy	22
3.2.3.3.2	Circular Dichroism Spectroscopy	22
3.2.3.4	Thermal analysis	23
3.2.3.5	Mechanical strength testing	23
3.2.3.6	<i>In vitro</i> bio-compatibility tests	
3.2.3.6.1	Hemo-compatibility test	24
3.2.3.6.2	<i>In vitro</i> Bio-activity assessment	24
3.2.3.6.3	<i>In vitro</i> Bio-degradation study:	25
3.2.4	<i>In vitro cell</i> study	
3.2.4.1	Cell proliferation assay	26
3.2.4.2	Cytoskeletal organization	26
3.2.4.3	Osteogenic differentiation potential assessment	
3.2.4.3.1	Alkaline Phosphatase Assay	27
3.2.4.3.2	Alizarin Red Staining	27
3.2.4.3.3	Osteocalcin and Run-x2 Expression	27
3.2.5	Statistical analysis	28

4. RESULTS AND DISCUSSION	
4.1 Effect of extraction procedure on keratin's stability	29
4.1.1 Protein Yield Quantification and SDS-PAGE	29
4.1.2 FTIR Analysis of extracted keratin	30
4.1.3 Circular Dichroism Spectroscopy Analysis	32
4.1.4 Particle size distribution and Zeta potential analysis	34
4.1.5 X-ray Diffraction analysis	35
4.1.6 <i>In vitro</i> Cellular Proliferation Assay	36
4.1.7 Cytoskeletal Organization	37
4.1.8 Conclusion	38
4.2 Synthesis and characterization of keratin based organo-apatites	39
4.2.1 Phase Analysis of synthesized organo-apatite	40
4.2.2 Morphological study	41
4.2.3 Functional Analysis	
4.2.3.1 FTIR Analysis	42
4.2.3.2 C.D Analysis	46
4.2.4 Thermal Analysis	47
4.2.5 Mechanical Strength Testing	48
4.2.6 <i>In vitro</i> Bio-compatibility studies	
4.2.6.1 Hemo-compatibility	50
4.2.6.2 <i>In vitro</i> Bioactivity assessment	51
4.2.6.3 <i>In vitro</i> Bio-degradation assessment	53
4.3 <i>In vitro</i> cell study and osteogenic differentiation potential of keratin based organo-apatites	
4.3.1 <i>In vitro</i> Cellular Proliferation through MTT	54
4.3.2 Cytoskeletal Organization	56
4.3.3 Osteogenic Differentiation Potential	
4.3.3.1 Alizarin red staining	57
4.3.3.2 Alkaline Phosphatase Assay	58
4.3.3.3 Osteocalcin and Run-x2 Expression	59

5. CONCLUSION	62
REFERENCES	64

LIST OF FIGURES

FIGURE	DESCRIPTION	PAGE NO.
3.1	Standard curve for protein estimation	17
3.2	Experimental set-up for organo-apatite synthesis by wet chemical co-precipitation	19
3.3	Organo-apatite nucleation and growth along the keratin fibrils	21
3.4	Uniaxially pressed organo-apatite samples for A- mechanical testing and for B- in vitro bioactivity and bio-degradation studies	23
4.1	SDS PAGE Pictogram; Lane-1 Molecular weight markers, Lane-2,3 Keratin isolated by Shindai method and Sodium Sulfide method respectively	29
4.2	FTIR Spectra between 4000-400cm ⁻¹ of keratin extracted by Sodium Sulfide Method and Shindai Method	31
4.3	Amide-I spectra and its 2 nd order derivative; Deconvoluted Amide-I spectra for Keratin extracted by sodium sulfide method	31
4.4	Amide-I spectra and its 2 nd order derivative; Deconvoluted Amide-I spectra for Keratin extracted by Shindai method	32
4.5	Far UV Circular Dichroism Spectra of keratin extracted by sodium sulfide and Shindai method	33
4.6	Particle size distribution obtained by Dynamic light scattering	34
4.7	A) Small angle x-ray diffractogram of Keratin extracted by Shindai and Sodium sulfide methods; B) Intensity vs. scattering vector plot from SAXS diffractograms of keratins extracted by Shindai and sodium sulfide method	35
4.8	Wide angle X-ray diffractogram of Keratin	36
4.9	In vitro Cellular Proliferation Assay through MTT assay	36
4.10	Cytoskeletal organization A) Tissue Culture Plate B) Shindai Method and C) Sodium Sulfide Method D) Box plot showing cell area indicating cell spreadability	37

4.11	Synthesized Keratin based Organoapatites showing greyish white appearance	39
4.12	X-ray diffractogram of hydroxyapatite and keratin based organoapatites	40
4.13	FESEM Images of A) pure hydroxyapatite synthesized without protein and organo-apatite composites B) HAP-K50, C) HAP-K75, D) HAP-K100, E) HAP-K125 and F) HAP-K150	42
4.14	FTIR spectra of keratin, pure hydroxyapatite and keratin based organo-apatite composites; a peak shift noticed in $1500-1700\text{cm}^{-1}$ suggesting possible interaction between the keratin and apatite crystals	43
4.15	Amide-I spectra and its 2 nd order derivative and corresponding Deconvoluted Amide-I spectra for A) Keratin protein B) HAP-K50 C) HAP-K75	44
4.16	Amide-I spectra and its 2 nd order derivative and corresponding Deconvoluted Amide-I spectra for D) HAP-K100 B) HAP-K125 C) HAP-K150	45
4.17	Far-UV CD spectra of the organo-apatite composites	47
4.18	TGA curve of keratin, pure hydroxyapatite and keratin based organo-apatite composites	47
4.19	Stress-strain curve for keratin based organo-apatites	49
4.20	FTIR Spectra of organo-apatites pellets after soaking in SBF for 14 days to assess the bio-activity	52
4.21	FTIR spectra between $1200-950\text{cm}^{-1}$ corresponding to carbonate and phosphate groups; A) HAP-K50, B) HAP-K75, C) HAP-K100, D) HAP-K125, E) HAP-K150 and F) Bioactivity assessment through $r_{c/p}$ ratio	52
4.22	Bio-degradation Study of organo-apatites	53
4.23	<i>In vitro</i> cellular proliferation through MTT assay	54
4.24	Phase contrast microscopy images at different time intervals while assessing cellular proliferation of ADSCs in TCP (Tissue culture plate) as control and in presence of hydroxyapatite and keratin based organo-	55

	apatite composites	
4.25	Cytoskeletal organization in presence of hydroxyapatite and keratin based organo-apatites; A) HAP, B) HAP-K50, C) HAP-K75, D) HAP-K100, E) HAP-K125, F) HAP-K150 and G) Box plot showing cell area indicating cell spreadability	56
4.26	Alizarin stained cells in presence of A) HAP, B) HAP-K50, C) HAP-K75, D) HAP-K100, E) HAP-K125 and F) HAP-K150	57
4.27	Alizarin red assay in presence of hydroxyapatite and organo-apatites	58
4.28	Alkaline phosphatase assay in presence of hydroxyapatite and organo-apatites	59
4.29	Osteocalcin expression after 21 days in presence of A) HAP, B) HAP-K50, C) HAP-K75, D) HAP-K100, E) HAP-K125, F) HAP-K150 and intensity/cell plot for osteocalcin expression	59
4.30	Runx2 expression after 7 days in presence of A) HAP, B) HAP-K50, C) HAP-K75, D) HAP-K100, E) HAP-K125, F) HAP-K150 and intensity/cell plot for Runx2 expression	60

LIST OF TABLES

TABLE	DESCRIPTION	PAGE NO.
2.1	Polymers used for organo-apatite synthesis	10
3.1	Extraction buffer composition for keratin extraction	16
3.2	Concentration of Keratin added for organo-apatite synthesis	20
3.3	Composition of Simulated Body Fluid	24
3.4	Composition of Phosphate Buffered Saline	25
4.1	Protein yield determined by Bradford's method	29
4.2	Percentage of secondary structures obtained from deconvoluted Amide-I spectra	32
4.3	Percentage of secondary structures obtained from far-UV C.D. spectra	33
4.4	Zeta potential and average diameter of keratin aggregates obtained by different methods	34
4.5	Concentration of Keratin added for organo-apatite synthesis	39
4.6	Percent Crystallinity and Crystallite size in 002 plane for different organo-apatites	41
4.7	Percentage of secondary structures obtained from deconvoluted Amide-I spectra	46
4.8	Percentage of hydroxyapatite present in the organo-apatite composites	48
4.9	Compressive strength and Young's modulus of keratin based organo-apatites	49
4.10	Percent porosity present in the organo-apatite uniaxially compressed pellets	50
4.11	Percent hemolysis of the hydroxyapatite and keratin based organo-apatites	51

LIST OF ABBREVIATIONS

°C	Celsius (Temperature)
ADSCs	Adipose Derived Stem Cells
ALP	Alkaline Phosphatase
ANNOVA	Analysis of Variance
BSA	Bovine Serum Albumin
cm	Centimeter
DMEM	Dulbecco's Modified Eagle Medium
FBS	Fetal Bovine Serum
FTIR	Fourier Transform Infrared Spectroscopy
g/L	Gram per liter
HAP	Hydroxyapatite
K Da	Kilo Dalton
LDV	Leucine-Aspartate-Valine
mg	Milligram
ml	Milliliter
MPa	Mega Pascals
MTT	3-(4,5-dimethylthiazol-2-yl)-2,5-diphenyltetrazolium bromide
nm	Nanometer
PBS	Phosphate Buffered Saline
RGD	Arginine-Glycine-Aspartate
Runx2	Runt-related transcription factor-2
SBF	Simulated Body Fluid
TGA	Thermo-gravimetric Analysis
v/v	Volume/Volume ratio
XRD	X-ray Diffraction

1. INTRODUCTION

1.1 BACKGROUND AND SIGNIFICANCE OF STUDY:

Bone is a highly structured and vascularized organ which has the primary function is to provide structural support and protection to the internal organs. In recent years much interest is gained in the area of curing critical sized bone defects which occur during primary tumor segmentectomy, trauma or accidental injury to the bone [1]. Though the bone has innate self-healing capability, the mending of critical size defects arising due to the mentioned causes puts up a real challenge. For treating such critical sized defects materials which are physically and chemically bio-mimetic material native to the bone such as organoapatites, self-assembled apatite on amphiphiles [2] and collagen-hydroxyapatite nanocomposites [3] are increasingly used. In order to develop a bone-biomimetic material, in this study keratin is chosen as the protein counterpart instead of collagen type-I, due to the various advantages and ease of extraction of keratin over collagen as a structural protein.

Keratins belong to a class of structural proteins found in external appendages such as hair, nails and in skin, which are cysteine rich and exhibit high mechanical strength due to the presence of large number of disulfide bonds [4]. In addition to this keratin is one of the most abundant proteins present in nature found in wool, hair, feather (poultry waste) etc. whose potential towards biomedical applications has to be exploited. For the study, human hair is chosen as the source of keratin because it is more autologous for *in vivo* application and human hair is deemed to be a waste and can be easily sourced from local saloons for developing the biomaterial. Keratin is found to be biocompatible and biodegradable polymer and is found to be a substrate for cell cultivation and improved cellular proliferation hence is a good candidate for application in tissue engineering.

In this study, keratin-hydroxyapatite organo-apatite is to be developed preferably mimicking the mineralized collagen of bone and its potential application in bone tissue engineering is studied through its material characterization and *in vitro* cell studies using Adipose derived Mesenchymal stem cells to assess its osteogenic differentiation potential.

1.2 ARCHITECTURE OF THE BONE:

Bone is a hierarchically ordered and highly vascularized tissue which is made up of 65% mineral phase, 25% organic phase and 10% water. The main mineral phase is hydroxyapatite, the organic matter is composed of collagen type-I protein and other non-collagenous protein such as bone sialoprotein, osteonectin, osteocalcin, fibronectin and osteopontin; and glycosaminoglycans (GAGs) and proteoglycans. The bone is formed by the directed growth of nano-scale ranged primary ceramic component - Hydroxyapatite ($\text{Ca}_{10}(\text{PO}_4)_6(\text{OH})_2$) on the triple helical collagen protein matrix (the principle protein in the bone), aligned parallel to the collagen fibril. Hydroxyapatite is one of the most stable calcium phosphate compounds with a hexagonal-dipyramidal crystallographic structure and has a Ca/P ratio of 1.67. Collagen is made up of majorly the repetitive triplet of amino-acids $-(\text{Glycine-Proline-Hydroxyproline})_n-$ which allows the primary polypeptide sequence to take up a triple helical conformation thus housing spaces between the helical conformation on to which the intrafibrillar crystals of hydroxyapatite nucleate from an amorphous precursor and form [5]. The Non-collagenous proteins (NCPs) help to monitor the nucleation and the growth of the hydroxyapatite crystals on the collagen fibrils.

The first level in the bone hierarchical architecture is the mineralized collagen. The mineralized collagen then aggregate and tend to form array patterns either uni-directionally (in case of the cortical bone) or in a disordered manner (in case of cancellous bone) [6]. This intricate array network forms ordered bundles, which include the lacunae where the osteocytes reside and the mineralized collagen fibril. The ordered bundle forms the osteon (functional cylindrical structures) which has the Haversian canal running amidst the lamellar matrix of arrayed mineralized collagen. Very fine channels arise from the lacunae towards the Haversian canal, thus making the compact bone a vascularized tissue. The final level in this hierarchical architecture is the classification of the mineralized tissue as either cancellous (porosity – 70 to 90%) or cortical bone (5 to 10% porosity). [2]

The bone is constantly remodeled by the aid of bone cells: osteoblasts which are responsible for the formation and regulation of bone extracellular matrix (osteoid, the bone extracellular matrix which consists of collagen, other non-collagenous proteins and polysaccharide), osteoblasts gets entrapped within the osteoid matrix and gets calcified as osteocytes which are responsible for

signaling during matrix signaling and resorption in response to mechanical stress and osteoclasts are responsible for the bone resorption. [7]

1.3 ORGANO-APATITES IN BONE TISSUE ENGINEERING:

Organo-apatites are a class of ceramic composite materials where hydroxyapatite crystals nucleate and grow in an organic polyelectrolyte or macromolecule (such as protein or polysachharide) media under a controlled physical and chemical environment. The important element is the macromolecule which helps in nucleating and regulating the size and the structure of the apatite crystals. The organo-apatites were found to have large surface area due to the slowly maturing nano-scaled apatite crystals within the macromolecular chains. Organo-apatites were first synthesized in 1980 by Stupp *et al*, in a poly-aminoacid (poly-L-lysine, poly-L-glutamate and poly-sodium-acrylate as macromolecules) media added with stoichiometric proportion of calcium and phosphate precursors to initiate nucleation and growth of apatite crystals [8]. Depending on the type of poly-aminoacid used the shape of the apatite varied as it was noticed with poly-L-lysine flat and thin apatite crystals were formed whereas with poly-L-glutamate, nanoscaled globular apatite crystals were formed. The organo-apatites were also found to be excellent in osteo-integration and osteo-regeneration when tested in canine cortical bone defects. Different synthetic and natural macromolecules have been tried after the advent of the first organo-apatite such as polyvinyl-alcohol, chitosan, bovine serum albumin and collagen type-1 based organo-apatites have been fabricated and have been used in bone tissue engineering applications.

1.4 KERATIN BASED ORGANOAPATITES:

Although there are many organo-apatites have been synthesized and its potential use in bone tissue engineering has been explored; only very few bone-mimetic organo-apatites with structural proteins such as collagen, silk fibroin and wool keratin have been fabricated till date. Collagen based organo-apatites were synthesized first by Kikuchi *et al* [3] in the year 2004 which paved way for the development of bone-mimetic organo-apatites for bone tissue engineering. However with the tedious process and cost involved in the collagen and fibroin extraction for the production of organo-apatites, an alternative structural protein such as keratin is exploited for the synthesis of bone-mimetic organo-apatites.

1.4.1 KERATIN:

Keratin is a fibrous structural protein found abundantly in nature. It is the principle structural protein found in the cytoplasmic epithelia and in the epidermal appendages such as in hair, nail, wool, hooves and claws in higher vertebrates. Keratin contains cysteine about 7-20% in the whole amino acid composition.[9] Keratins are classified as hard and soft keratins. The hard keratin falls into two major categories i.e. α -keratin (found in hair, nail, and hooves of mammals) and β -keratin (found in feathers, scales of reptiles). The soft keratin or the cytokeratin are those that are found inside the cytoplasmic skeleton of epithelial tissues. [10]

1.4.2. STRUCTURE OF HARD-ALPHA-KERATIN:

The hard α -keratin found in human hair consists of two majors subgroups namely, the Intermediate filament (IFs) or the α -keratins and the Keratin matrix associated proteins (KAP). [11] The intermediate films (IFs) are the main structural entity of the hair keratin predominantly composed of α -helical structures that consists of two chains type-I (acidic) and type-II (neutral/basic) polypeptide chains. These IFs are low sulfur content containing components of keratin and they assemble into heterodimer by antiparallel manner. [12] The KAP are the high sulfur containing globular subunit of the keratins, which help to keep the keratin intact inside the hair sheath by compactly binding with the intermediate filaments.[13] It consists of two components, a high sulfur containing domain (10-30kDa) and high tyrosine containing proteins (6-9kDa).[14] The hard keratin are assembled by interaction of two helical type-I and type-II polypeptide chains of intermediate filaments which forms the heterodimers. The heterodimers dimers interact by intermolecular hydrogen bonding forming octamers and consequently form the cylindrical unit length filament of hair sheath. The unit length filaments are held tightly by the matrix associated protein and which in turn form the tertiary structure of the hair fibril. [15]

1.4.3. KERATIN AS IDEAL BIO-POLYMER FOR ORGANO-APATITE SYNTHESIS:

The hard alpha keratin found in hair is an ideal candidate for synthesis of bone-mimetic organo-apatite, since it being a majorly helical protein aiding a suitable aboard for the nucleation of the apatite crystals. Keratin possesses key amino acid motifs such as RGD (arginine-glycine-aspartate) and LDV (leucine-aspartate-valine) [16] and EDS (glutamate-aspartate-serine) to which $\alpha 5$, $\alpha 4$ integrin receptor family binds and hence enhancing its cell adhesion

properties.[17, 18] In addition to this the keratin supports cellular proliferation, where it is found to enhance cellular proliferation of mouse fibroblasts in keratin coated plates than in glass or collagen coated plates [19] and similar inference is seen in human hair keratin based hydrogels which support fibroblast attachment and proliferation.[20] Keratin hydrogels were also found to be helpful in wound healing by favoring the re-epithelialization as keratin was found to be mitogenic for keratinocyte, fibroblast and endothelial cells thus helping in rapid wound healing.[21, 22] Hence the use of keratin from human hair for the development of bone-mimetic organo-apatite seems productive due to the advantages of keratin over other structural proteins used till date.

1.5 OBJECTIVES:

1. To determine the best method for the extraction of keratin from human hair, for use in the development of organo-apatites
2. To synthesize keratin/hydroxyapatite bone-mimetic organo-apatites with varying concentrations of keratin
3. To study the physical and chemical properties of the synthesized bone-mimetic organo-apatites
4. To perform *in vitro* cell study on the synthesized bone-mimetic organo-apatites and to assess its differentiation potential using human Adipose Derived Mesenchymal Stem cells (hADSCs)

2. LITERATURE REVIEW

2.1 EXTRACTION OF KERATIN FROM HUMAN HAIR:

Keratin can be extracted either by oxidative or reductive methods and the keratin obtained is termed as keratose or kerateine respectively by the method that is used. The keratose are more soluble forms of keratin in which the disulfide linkages present in keratin are converted to sulfonic acid groups [15] whereas the keratiene are relatively less soluble forms where the disulfide bonds are broken down to thiol groups. Keratoses are generally extracted with the aid of oxidizing agents like peracetic acid, while keratiene are obtained through the help of reducing agents such as mercaptoethanol, thioglycolic acid sodium sulfide etc. The keratin is extracted from the cortex of the hair fibril or any other epidermal appendages such hoof, feather etc., through these above mentioned denaturants which break the hydrogen bonds and mainly the disulfide linkages to obtain a soluble form of keratin in the extraction buffer. After removal of the denaturants the keratin reverts back to its original α -helical conformation as postulated by Anfinsen (1950), by the virtue of the details present in amino-acid sequence. [23]

2.1.1 EXTRACTION OF KERATOSE:

Alexander and Earland (1950) used 2% peracetic acid and the protein fraction was neutralized with NaOH [24]. The protein fraction contained both the IF and KAP regions. The protocol itself is a benchmark in extracting keratose from wool, hair and has been used till date. Haylett *et al*, (1963) extracted oxidized keratin from wool with the aid of performic acid in pyridine-acetate buffer (pH 6.0). Analysis of the extracted fraction of the keratose revealed that the fractions contained mostly high sulfur containing residues indicating the extraction was more effective in isolating the keratin associated proteins [25]. O'Donnell *et al*, (1963) used performic acid for keratin extraction but the dialyzed protein fraction after acid treatment was exposed to 0.1M potassium sulfate, whereby the alkaline pH helped in isolation of low-sulfur containing regions of keratin (IF) and thus aiding in isolating the keratin intermediate filaments and keratin associated proteins in oxidized form [26].

Mark E. Van Dyke *et al*, (2000-2015) pioneered the work in keratin based biomaterials for various tissue engineering applications such as use in wound healing, bio-ceramics for bone regeneration etc. Burnett *et al* (2015) used hydrogen peroxide for the extraction of keratose from

human hair [27]. The keratose fractions obtained through oxidative method obtain keratin where the disulfide linkages are made into sulfonic acid group [15]. The peracetic acid used conventionally gets hydrolyzed into acetic acid and hydrogen peroxide. The hydrogen peroxide is a strong oxidant which permanently modifies amino acids like methionine, cysteine and tryptophan into sulfonic acid, sulfoxide and sulfone respectively [28]. The keratose based systems are still finding application in controlled drug release, as in case of controlled release of ciprofloxacin done by Justin Saul *et al*, (2011) whereby the ciprofloxacin interact electrostatically with the modified amino acid residues and gets released in controlled manner with degradation of the keratose hydrogel [29].

Oxidative method of extraction though it yields more soluble forms of keratin the protein is modified irreversibly and the biological properties and its mechanical properties are altered. The keratose obtained are non-disulphide crosslinkable and can easily undergo hydrolytic degradation due to the polarized back-bone (due to the presence of sulfonic acid residues) and therefore it is found to undergo rapid deterioration *in vivo* applications [11].

2.1.2 EXTRACTION OF KERATIENE:

Corfield *et al* (1958) used 8M urea and 5% 2-mercaptoethanol in 25mM Tris-HCl (pH 9.5) for removal hard α -keratin from human hair samples in forensic studies [30]. Researchers conventionally used this protocol for extraction of keratiene from hair since 1960. Van Dyke *et al* (2010) used thioglycolic acid for reduction of disulfide linkages and extraction of reduced form of keratin from human hair for medical preparation of keratin for development of wound healing and blood clotting aids [22]. However the yield of keratin by this method is relatively low when compared to the mercaptoethanol method.

Akira Nakamura *et al* (2002) developed an extraction protocol for isolating reduced form of keratin from human hair which is the most commonly followed (since 2002) protocol for extraction of keratiene. The name Shindai is derived from the university from which the extraction procedure was developed, Shinshu University [14]. In the extraction protocol, 2.6M Thiourea, 5M urea and 5% 2-mercaptoethanol Tris-HCl (pH 8.5) were used to break the hydrogen bonds and reduce the disulfide bridges respectively. The Shindai method was found effective with extracting keratin from chicken feather, human nail, rat hair and wool.

Andrew J. Poole *et al*, (2011) used sodium sulfide to extract keratiene from chicken feather. The sodium sulfide is relatively less corrosive denaturant and can be easily removed from the extraction buffer by dialysis. It was noted in the study for the ease of extraction and for large scale production of keratin from waste chicken feather, this method was applied. The sodium sulfide reacts with water to form reactive hydrosulfide anion and hydroxyl ions. The hydrosulfide reduces the disulfide linkages present in the keratin chains, and the high pH is maintained by the hydroxyl ion which helps to break down the hydrogen bonding [31].

Scheme for disulfide bond reduction through sodium sulfide:



Scheme for disulfide bond reduction through 2-mercaptoethanol:



The reduced keratin obtained is less polar than the keratose hence it is relatively less readily soluble in water. The keratiene material can easily be cross-linked through oxidative methods to form highly crosslinked hydrogels or films and they are much stable at high pH and temperature thus having better persistence against degradation suitable for *in vivo* applications. It has been demonstrated that keratiene can be successfully harnessed for supporting cell growth, where fibroblast cells cultivated in keratiene hydrogels were found to proliferate better than in collagen hydrogels [20], and films based on keratiene were able to support keratinocytes adhesion and proliferation [32] for wound healing applications.

2.2 EFFECT OF EXTRACTION PROCEDURE ON PROTEIN FOLDING:

For extraction of keratin from human hair generally denaturants are used to disassociate the keratin from the internal hair fibrils. Since α -keratin of the hair contains about 7-20% cysteine residues which give it the mechanical strength as a structural protein, the disulfide linkages have to be reduced in order to isolate the keratin in solution. However based on the denaturant used, the ability of the protein to refold to its original conformation is dependent. Often the proteins aggregate and form inclusion bodies. Lau *et al* (1984) synthesized poly-heptapeptides which were 100% of alpha helical conformation which were subjected to different denaturants and retrieved and their ability to refold back in solution was studied. The hepta-peptides lost 30% of

its alpha conformation when exposed to 6M urea and then removed suggesting that urea has permanent effect in disrupting the hydrophobic residues and in turn the alpha helical conformation is lost [33].

Dunbar *et al* (1997) studied the effect of guanidium chloride and urea on the denaturation of dihydrofolate reductase (DHFR) and ribonuclease-A (RNase). It was observed through NMR and x-ray diffraction studies that these denaturants hinder the hydrogen bonding and critically reduce the overall thermal factor leading to thermodynamically unstable aggregation of the proteins under study [34]. It was observed by Clark (2001) that with high denaturant concentration such as with 2M urea (pH 12.5) the proteins undergo irreversible chemical modification resulting in losing their native conformation [35].

Middelberg *et al* (2002) observed in refolding of inclusion bodies in *Escherichia coli*, in concentrations of greater than 500mM dithiothreitol (DTT) led to malformed disulfide linkages [36]. The 2-mercaptoethanol which is also a reducing agent like DTT helps to cleave the disulfide bridges and is vastly used in keratin preparation from hoofs, feather and hair [37]. In certain extraction procedures instead of 2-mercaptoethanol, sodium sulfide or thioglycolic acid is also used. Rao *et al* (1958) studied the effect of disulfides and sulfides on the reduction of the cysteine residues. In the presence of excess sulfide the cysteine residues reacts and produces two cysteinate ions and disulfide or polysulfide ions. These cysteinate ions and polysulfide ions when the brought down to lower pH from alkaline pH forms disulfide crosslinks automatically. Though there is no study till now carried out on how the extraction procedure involving 2-mercaptoethanol and sodium sulfide has an effect on the extracted protein's folding.

2.3 SYNTHESIS OF ORGANO-APATITES:

Organo-apatites were first synthesized in 1980s by Stupp *et al*, which are a class of bio-ceramic material. These materials are formed by nucleation and development of apatite in media containing poly(amino-acids) or polyelectrolytes under strict environmental, temperature, and pH control. The macromolecules used by Stupp *et al* to combine the organo-apatites included poly(L-lysine), poly(L-glutamic corrosive), and poly(sodium acrylate). The synthesized organoapatites were found to contain large surface area morphologies with little crystallites which develop gradually in the supra-molecular network. The natural macromolecules are

thought to impel nucleation of apatites and also regulate their size. [8] Since the first synthesis of organo-apatite several macromolecules like such as polyvinyl-alcohol, chitosan, bovine serum albumin and collagen type-1 based organo-apatites have been fabricated and have been used in bone tissue engineering applications. Below is listed the account of different types of organo-apatites synthesized using different polymer network over the period of time:

Table – 2.1: Polymers used for organo-apatite synthesis

S.NO.	POLYMER USED	OUTCOME	REFERENCE
1.	Poly (L-lysine) and Poly (L-glutamic acid)	Poly (L-lysine) formed large and thin crystals, while poly (L-glutamic acid) formed globular nano-crystals	Stupp <i>et al</i> (1992) [8]
2.	Atelocollagen	Formation of apatite crystals in 1-5% atelocollagen solution for the use in bone filling cement was first demonstrated	Miyamoto <i>et al</i> (1998) [38]
3.	Collagen	The collagen-apatite (non-stoichiometric) was used for delivery of drugs such as norfloxacin and ciprofloxacin for control of bone infection	Martins VC <i>et al</i> (2000) [39]
4.	Porcine atelocollagen	20µm bundle of collagen-HAP organo-apatite, 50nm sized blade shaped HAP crystals were deposited along the collagen fibril oriented in the c-axis of HAP	Kikuchi <i>et al</i> (2000) [40]
5.	Bovine Serum albumin (BSA) and Polyvinyl Alcohol (PVA)	Microporous and nanosized hydroxyapatite crystals (5-40nm) were synthesized in a controlled fashion along the synthetic and bio-polymer network	Sinha A <i>et al</i> (2002) [41]
6.	Bovine Serum albumin (BSA) and Collagen	Rhombohedral shaped apatite crystals were formed in the nan-cavities of globular BSA protein, while mesoporous sheet like apatite crystals were formed over helical cavities of the collagen matrix	Nayar <i>et al</i> (2003) [42]
7.	Polyvinyl Alcohol	Wide array of morphologies from spherulites	Sinha A <i>et al</i>

	(PVA)	to helical structures of apatite were synthesized by varying the polymer concentration used as a template for apatite growth and nucleation	(2003) [43]
8.	Collagen Type-I	Rod shaped HAP crystals of size 50nm were formed along the collagen fibril	Carvallo <i>et al</i> (2004) [44]
9.	Collagen Type-I	Collagen type-I containing an alkaline phosphatase enzyme was added to aqueous solution of calcium ions and phosphate ester. The ALPase cleaved the phosphate ester to release the phosphate ions for calcium phosphate to nucleate and mineralize along the collagen fibril	Yamauchi <i>et al</i> (2004) [45]
10.	Alginate	Poorly crystalline apatite crystals were deposited heterogeneously along the ribbon shaped polymer network	Tampieri <i>et al</i> (2005) [46]
11.	Silk sericin	Heterogenous nucleation and growth of HAP spherical crystals where formed from metastable calcium and phosphate precursor solutions along the β -pleated sericin fibrils	Takeuchi <i>et al</i> (2005) [47]
12.	Collagen Type-I	Blade shaped HAP crystals of size 50nm were formed along the collagen fibril	Wahl <i>et al</i> (2006) [48]
13.	Recombinant Collagen	Recombinant acidic collagen helped in directed growth of nano-apatite for the formation of mineralized collagen aligned parallel to each other	Zhai <i>et al</i> (2006) [49]
14.	Chitosan	Amorphous calcium carbonate deposition on the chitosan polymer network in the presence of an additive (poly acrylic acid)	Zhang <i>et al</i> (2006) [50]
15.	Multi-walled Carbon nanotubes	Multi-walled carbon nano-tubes with 40nm bamboo periodic microstructure was used as network for housing the nucleation and growth	Liao <i>et al</i> (2007) [51]

		of spindle shaped hydroxyapatite of varying crystal size ranging between 10-40nm	
16.	Collagen Type-I and Silk fibroin	Bi-template based HAP deposition on two polymers was carried out resulting in needle-like HAP of 53.5 nm in size deposited within the polymer intertwined network	Wang <i>et al</i> (2009) [52]
17.	Polyvinyl Alcohol (PVA)	HAP nano-rods of length 20-120nm and width of 10-30nm were formed within a PVA network	Man Kim (2010) [53]
18.	Porcine dermal acellular matrix collagen	HAP nano-crystals were formed in porcine acellular dermal matrix, showing improved osteo-conductivity and bioactivity	Zhao <i>et al</i> (2011) [54]
19.	Wool keratin	Irregular rod shaped HAP localized along the keratin fibril in random fashion was formed	Li <i>et al</i> (2012) [55]
20.	Alginate, collagen type-I	A bi-template method HAP nucleation and growth of HAP crystals was carried out	Akinori <i>et al</i> (2012) [56]

Thus a handful of synthetic and natural polymers have been used for the synthesis of organo-apatites and have been successfully used in bone tissue engineering. Although only very few bone-mimetic organo-apatites with structural proteins such as collagen, silk fibroin and wool keratin have been fabricated till date. Collagen based organo-apatites were synthesized first by Kikuchi *et al* [3] in the year 2004 which paved way for the development of bone-mimetic organo-apatites for bone tissue engineering. However with the tedious process and cost involved in the collagen and fibroin extraction for the production of organo-apatites, an alternative structural protein such as keratin from human hair is exploited for the synthesis of bone-mimetic organo-apatites in this study.

2.4 OSTEOGENIC DIFFERENTIATION OF ADULT STEM CELLS:

For the osteogenic differentiation of Adult Stem Cells (ADSCs), (wherein in this study Adipose derived stem cells were used) a cocktail mixture of β -glycerophosphate, dexamethasone and ascorbic acid supplemented in complete media (DMEM with 10% FBS and antibiotics) is used

[57-60]. Each of the three constituent helps in induction of osteogenic differentiation through different molecular pathway crucial for osteogenesis. Tenenbaum *et al* (1985) first optimized the dexamethasone concentration to be around 100nM to aid the chick periosteal explants towards osteogenic lineage [61]. It was also reported that dexamethasone helps to prevent apoptosis in differentiating stem cells [62]. Dexamethasone helps to activate the early differentiation marker – Runx2 (Runt related transcription factor-2) through WNT- β -catenin mediated pathway [58] and by upregulation of MAPK-1 (Mitogen Activate Protein Kinase-1) which in turn activates the Runx2 expression [63]. In addition to this dexamethasone also modulates the ER- α (Estrogen receptor) and osteopontin expression. [64]

β -glycerophosphate is generally used in concentration of 10mM for osteogenic induction [59]. β -glycerophosphate serves as the phosphate precursor for the formation of hydroxyapatite for differentiating cells and also the in-organic phosphate from the β -glycerophosphate helps as a transcription factor for transcribing key differentiation markers like osteopontin and BMP-2 (Bone morphogenetic Protein), a key cytokine regulating the osteogenic differentiation [58]. Choi *et al* (2008) studied the effect of ascorbic acid on the proliferation and differentiation of Mesenchymal stem cells at a concentration range between 0-500 μ M. It was observed that within a range of 5-250 μ M concentration of ascorbic acid stimulated the formation of extra-cellular matrix components like collagen and glycosaminoglycan thus aiding in the differentiation process [65]. Ascorbic acid is an important co-factor for the enzymes prolyl hydroxylase and lysyl hydroxylase which is involved in the hydroxylation of the proline and lysine residues of the collagen-I [66, 67]. The collagen-I is an important extracellular matrix protein which is formed by the hydroxy proline and hydroxy stabilized triple helix conformation of the protein. The secreted collagen matrix in turn helps to upregulate the Runx2 expression through the α 2 β 1 integrin binding and β -catenin mediated pathway. [58]

2.5 KERATIN AND OSTEOGENIC DIFFERENTIATION POTENTIAL:

Keratin based biomaterials are known to support cell proliferation and cell attachment and hence serve as a good platform for fabricating biomaterials for tissue engineering application. The use of keratin based biomaterials for bone tissue engineering is being exploited in the recent years. Tachibana *et al* (2005) fabricated keratin-hydroxyapatite sponges in order to create a bone-mimetic scaffold, which were assessed using MC3-T3-E1 (pre-osteoblast cell line). The

composite sponges were helpful in osteogenic differentiation which was evident from the alkaline phosphatase expression, which is a key early osteogenic marker [68]. Tachibana *et al* (2006) were successful in developing carboxylated keratin sponge based scaffold for bone tissue engineering. The carboxylated keratin was helpful in mimicking the matrix- γ -carboxy glutamic acid protein which helps in osteoblast calcification; in addition to this the carboxylated-keratin is helpful in harboring the BMP-2 (a cytokine helpful in osteogenic differentiation). The carboxylated keratin sponges adsorb the BMP-2 and helps in controlled delivery of the cytokine when the composite sponge was used for bone tissue engineering applications.

Li *et al* (2009) fabricated keratin/PLLA based electrospun matrix for bone tissue engineering application which was assessed using osteoblast cell line. The keratin/PLLA composite matrix were found to induct osteogenic differentiation and provide a conducive environment for cell attachment and growth when compared to control PLLA network. This was mainly due to the presence of keratin in the composite network, proving that the keratin is osteoconductive [69]. Dias *et al* (2010) conducted an *in vivo* study with reconstituted keratin with 40% hydroxyapatite composites fabricated through compression molding technique. The *in vivo* study was conducted in ovine system, and it was found that composites showed superior mechanical stability and better osteogenesis by 8-10 weeks after implantation and revealed full osseo-integration within 12-18 weeks [70]. Thus keratin in addition to its ability to promote cell adhesion and proliferation is also found to be osteoconductive, which is very suitable for the purpose of preparation of organo-apatites in this study.

3. MATERIALS AND METHODS

3.1 MATERIALS:

3.1.1 EXTRACTION OF KERATIN:

Sodium Do-decyl Sulfate, chloroform, methanol, urea, thiourea, sodium sulfide, acrylamide, bis-acrylamide and TEMED were obtained from Rankem, India. Chloroform, methanol, Tris-HCl, were obtained from HiMedia, India. Orthophosphoric acid (85%), coomassie brilliant blue, glacial acetic acid were obtained from Merck, USA. Dialysis membrane (D9562) was obtained from Sigma Aldrich, USA. Mercaptoethanol was obtained from Loba Chemie.

3.1.2 SYNTHESIS OF KERATIN BASED ORGANO-APATITES:

Calcium hydroxide, sodium chloride, sodium hydroxide, sodium bicarbonate, calcium chloride, potassium chloride, disodium hydrogen phosphate, magnesium chloride, sodium sulfate were obtained from HiMedia, India. Orthophosphoric acid and ammonia were purchased from Merck, USA.

3.1.3 CELL CULTURE STUDY:

Dulbecco's Low glucose media, 100X antibiotic-antifungal mix, Fetal Bovine Serum, Trypsin-EDTA 100X (0.5%), L-Ascorbic acid, Dexamethasone, MTT were purchased from HiMedia, India. β -glycerophosphate, dimethyl sulfoxide (DMSO) were obtained from MP Biomedicals. Alizarin red was purchased from Sigma Aldrich, USA. All the fluorescent dyes mentioned in the procedures were procured from Invitrogen Life Technologies, USA.

3.2 METHODS:

3.2.1 EXTRACTION OF KERATIN FROM HUMAN HAIR:

3.2.1.1 PROCESSING OF HUMAN HAIR:

Human hair was collected from local barber shop and rinsed thoroughly with water. It was then soaked 0.5% SDS and washed to remove the detergent using distilled water and dried in room temperature. Lipids were removed by soaking the hair in 2:1 (v/v) chloroform: methanol. The

solvent was filtered out and the hair was dried in room temperature to remove any residual solvent.

3.2.1.2 EXTRACTION PROTOCOLS FOR HUMAN HAIR KERATIN:

The lipid free hair is cut into small pieces; 5g of the hair was immersed in 100mL of the extraction buffers and incubated at the mentioned temperature and time as seen in Table-3.1. After the extraction, the hair is filtered and the buffer was dialyzed against distilled water for 3 days with intermittent change of water for 3 days to remove the denaturing agents. The dialysate contains aqueous suspension of protein which is concentrated using rotary vacuum drier and lyophilized for future use. (The dialysate can also be stored in -20°C which is stable for a month and thawed when required)

The extraction of keratin from human hair was done by two procedures namely, Shindai method [14] and sodium sulfide method [20]. The extraction buffers composed of:

Table - 3.1: Extraction buffer composition for keratin extraction

Conditions	Shindai Method	Sodium Sulfide Method
Extraction Buffer composition	5M Urea 2.6M Thiourea 5% v/v Mercaptoethanol 25mM Tris HCl (pH 8.5)	0.125M Sodium Sulfide
Extraction Temperature	50°C	40°C
Time Duration	72 hours	4 hours

3.2.1.3 PROTEIN QUANTIFICATION BY BRADFORD'S ASSAY:

The keratin extracted by each method was quantified by Bradford's method [71] with Bovine Serum Albumin as the standard. The 5X Bradford reagent was prepared as follows: 25mg coomassie brilliant blue dissolved in 12.5ml of methanol to which 25ml of 85% orthophosphoric acid was added (dark red colour formation noticed). The solution was diluted by adding 50 ml of water. 87.5 ml of this solution was then filtered and stored in brown bottle at 4°C. The working

reagent is 1X, which was prepared by diluting the 5X reagent with distilled water. For 50 μ l of sample, 2.5ml of 1X Bradford's reagent was used for estimation, incubated in dark for 10 minutes and the absorbance was measured at 595nm using UV-Visible spectrophotometer.

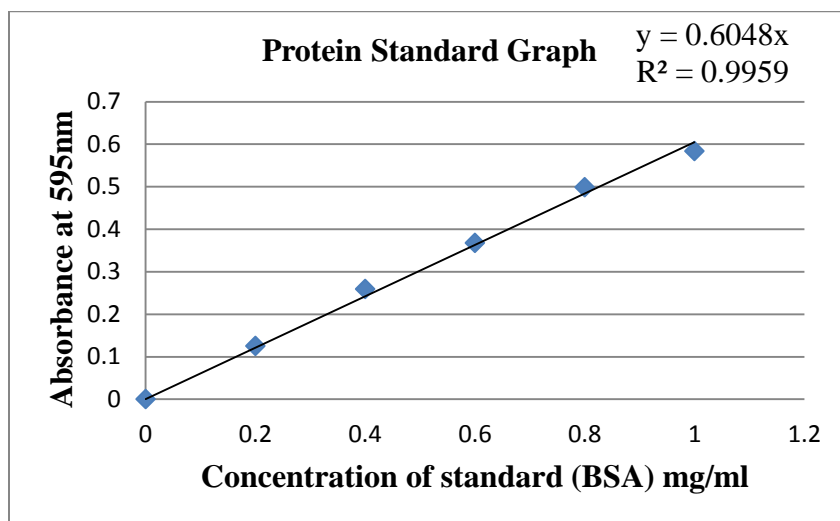


Figure – 3.1: Standard curve for protein estimation

From the standard curve the quantity of protein present after extraction procedure by each method was estimated, with the experiments conducted in triplicates.

3.2.1.4 SDS-POLYACRYLAMIDE GEL ELECTROPHORESIS:

The extracted protein fraction was resolved in 15% SDS-Poly acrylamide gel by using method of Laemmli [72] loading 100 μ g of protein per well. The gels were stained with 0.1% coomassie brilliant R-250, 40% methanol and 10% glacial acetic acid for 1 hour and destained using 10% methanol and 7% glacial acetic acid.

3.2.1.5 CHARACTERIZATION OF EXTRACTED KERATIN:

3.2.1.5.1 Fourier Transform Infrared Spectroscopy:

Attenuate total reflectance Fourier transform infrared spectroscopy (ATR-FTIR) was performed using Alpha-E ATR-FTIR Bruker Spectrometer, Germany. Protein samples in aqueous solution (5mg/ml) were placed in ZnSe plate for analysis. A total of 25 scans with a resolution of 8 cm^{-1} were done in the range of 400-4000 cm^{-1} .

The Amide-I spectra of the keratin extracted were deconvoluted by taking second order derivative of the Amide-I region and fitting multiple peaks by Gaussian peak fitting, for determining the secondary structures of the protein.

3.2.1.5.2 Zeta potential analysis and Dynamic Light Scattering:

The particle size distribution of the keratin extracted by different method and the zeta potential were measured using Malvern Zetasizer Nano ZS instrument. The concentration of protein was kept at 0.1mg/mL for the protein in milli-pore water.

3.2.1.5.3 Circular Dichroism Spectroscopy:

Far UV C.D spectra (190nm to 250nm) of the aqueous protein solution of concentration 0.1mg/ml was done in a 1mm path-length cuvette in Jasco-J1500 (JASCO, Japan) dichrometer. A total of 3 accumulations were taken at a scan rate of 100nm/min with 0.25s time constant at 25°C. The secondary structures were determined using CONTIN algorithm. The C.D. spectra was reported as mean residue molar ellipticity θ_{mrw} (degrees.cm².dmol⁻¹) as,

$$\theta_{mrw} = \theta \cdot mrw / 10 \cdot d \cdot c$$

Where θ is observed ellipticity in degrees, mrw is mean residue molar molecular weight in g/mol, d is pathlength of cell in cm, c is the concentration of protein in g/ml. The far-UV CD spectra were analyzed using the Jasco's secondary structure estimation software using Yang's reference set as reference spectra.

3.2.1.5.3 X-ray diffraction:

Small angle X-ray scattering was done using Rigaku Ultima-IV multipurpose X-ray diffractometer, with the aqueous protein solution of concentration 5mg/mL taken in a quartz capillary of 1mm thickness, between 0.8° to 3°, with a step size of 0.03 and a scan rate of 0.1°/minute. The scattering vector (s) was calculated,

$$s = 1/d$$

where, d is the Bragg's d spacing. Wide angle X-ray Diffraction of the lyophilized protein sample was done to determine the qualitative phase content between the ranges 3° to 60° with a

step size of 0.03 at a scanning rate of 5°/minute in Rigaku Ultima-IV multipurpose X-ray diffractometer.

3.2.2 SYNTHESIS OF KERATIN BASED ORGANO-APATITES:

The organo-apatites were synthesized by using wet chemical co-precipitation method. The inorganic precursors used were calcium hydroxide ($\text{Ca}(\text{OH})_2$) and ortho-phosphoric acid (H_3PO_4). The organic supermolecular bio-polymer network to house the hydroxyapatite nucleation and growth is the keratin obtained through sodium sulfide method. The Ca:P molar ratio was maintained at 1.67, to aid the formation of hydroxyapatite within the supramolecular keratin fibrils. The pH was maintained around 10 to 11 using NH_4OH and the temperature was maintained at 40°C.



Figure – 3.2: *Experimental set-up for organo-apatite synthesis by wet chemical co-precipitation*

The protein in different concentrations was dissolved in 0.06M orthophosphoric acid and it was added drop by drop to 0.1M calcium hydroxide, such that hydroxyapatite is formed over the fibrous protein. The negative charge bore on the protein act as the nucleation point where

calcium ion binds and the growth of hydroxyapatite occurs. Similarly, neat hydroxyapatite without any protein was also synthesized as control.

The chemical scheme for hydroxyapatite synthesis is as follows:



The following table shows the keratin concentration taken for the organo-apatite synthesis and the respective denominations given:

Table – 3.2: Concentration of Keratin added for organo-apatite synthesis

S. No.	Protein added in 0.06M H ₃ PO ₄	Composite denomination
1.	2.50 g/L	HAP-K50
2.	3.75 g/L	HAP-K75
3.	5.00 g/L	HAP-K100
4.	6.25 g/L	HAP-K125
5.	7.50 g/L	HAP-K150

The proposed mechanism as seen in Figure-3.3 is that the negatively charged carboxyl groups in the amino-acid side chains of the peptide acts as nucleation points to which the phosphate and calcium precursors bind and apatite nucleation starts, followed by the growth of the apatite crystal.

After synthesis the organo-apatite formed was aged for 24 hours. The resultant precipitate was centrifuged and collected. The collected precipitate was washed thrice with distilled water to remove any residual unbound protein and precursors. The precipitate was freeze dried and the fine powder collected was stored in -20°C for future use.

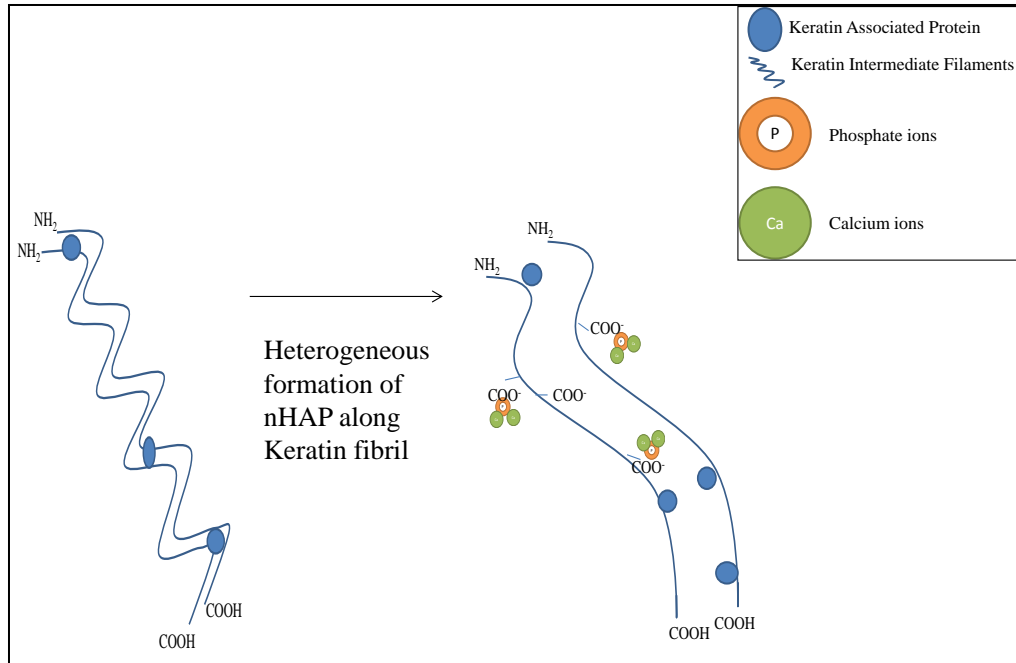


Figure – 3.3: *Organo-apatite nucleation and growth along the keratin fibrils*

3.2.3 CHARACTERIZATION OF ORGANO-APATITES:

3.2.3.1 X-RAY DIFFRACTION:

X-ray Diffraction of the organo-apatite and hydroxyapatite (control) was done to determine the qualitative phase content between the ranges 5° to 60° with a $\text{Cu-K}\alpha$ as radiation source with a step size of 0.05 at a scanning rate of $5^{\circ}/\text{minute}$ in Rigaku Ultima-IV multipurpose X-ray diffractometer operated at 35kV and 30A. The phase and Crystallinity was compared and identified using reference data set from JCPDS (Joint Commission for Powder Diffraction Studies) database using X'pert high score software.

The Percent Crystallinity was calculated using the formula:

$$\text{Percent Crystallinity } (X_C) = (1 - v_{(211/300)} / I_{300}) * 100$$

Where,

$v_{(112/300)}$ - intensity of hollow between peaks 112 and 300

I_{300} - intensity of peak 300

The crystallite size along the axis perpendicular to the c-axis from the peak corresponding to 002 miller indices, which is the highest intensity peak helps to determine the crystallite size. It can be calculated as follows:

$$\text{Crystallite size} = 0.9\lambda/\beta\cos\theta$$

Where,

λ – 0.154 nm

β – FWHM – Full width half maxima of the peak corresponding to 002 (in radians)

θ – diffraction angle

3.2.3.2 FIELD EMISSION SCANNING ELECTRON MICROSCOPY:

The morphological analysis of the organo-apatites was done using Nova NanoSEM 450/ FEI, equipped with high current Schottky gun with a beam landing energy of 50 V and capable of resolution of 1.4 nm at 1 kV without beam deceleration. The dried organo-apatites were coated with gold prior to analysis.

3.2.3.3 FUNCTIONAL ANALYSIS:

3.2.3.3.1 Fourier Transform Infrared Spectroscopy:

Fourier transform infrared spectroscopy was performed using Shimadzu IRAffinity instrument. Prior to scanning the samples were mixed with KBr powder (1:99) and pressed to 10mm diameter discs. The pressed disc was scanned in the range of 400-4000 cm^{-1} with KBr as background. The Amide-I spectra of the keratin extracted were deconvoluted by taking second order derivative of the Amide-I region and fitting multiple peaks arising as Gaussian peaks. The percentage of secondary structures present was calculated based on the area under the curve assigned for each curve.

3.2.3.3.2 Circular Dichroism Spectroscopy:

Far UV C.D spectra (190nm to 250nm) of the sonicated organo-apatite and hydroxyapatite samples for concentration of 1 mg/ml were done in a 1mm path-length cuvette in Jasco-J1500 (JASCO, Japan) dichrometer. A total of 3 accumulations were taken at a scan rate of 100nm/min

with 0.25s time constant at 25°C. The C.D. spectra is reported as mean residue molar ellipticity θ_{mrw} (degrees.cm².dmol⁻¹) as,

$$\theta_{\text{mrw}} = \theta \cdot \text{mrw} / 10 \cdot d \cdot c$$

Where θ is observed ellipticity in degrees, mrw is mean residue molar molecular weight in g/mol, d is pathlength of cell in cm, c is the concentration of protein in g/ml.

3.2.3.4 THERMAL ANALYSIS:

The weight change of the organo-apatite samples were detected by thermo-gravimetric analysis (TGA) using Netzsch, Germany, STA449C/4/MFC/G instrument, under an argon atmosphere placed in alumina crucibles. The samples were weighed between 10 and 15 mg. The change in weight was measured between room temperature 25°C to 1200°C, at the rate of 10°C/minute. The data was acquired for every 0.05 seconds.

3.2.3.5 MECHANICAL STRENGTH TESTING:

For the purpose of mechanical testing, the organo-apatites synthesized were pressed into pellets by uniaxial compression using a 12mm die at 1.27 MPa for 80 seconds. The pellets made were of 11-12mm in diameter and a height of 6-7mm. The compressive strength of the pressed pellet for each organo-apatite sample was done in duplicates using H10 KS Tinius Olsen Universal testing machine with a load cell of 10KN and with a cross-head speed of 2mm/minute.

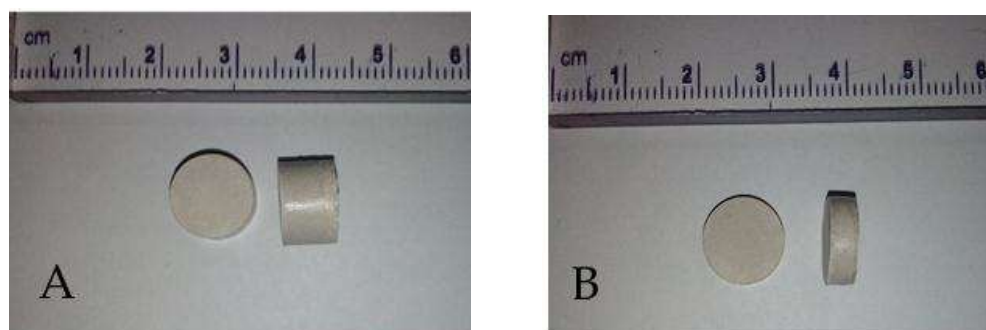


Figure – 3.4: Uniaxially pressed organo-apatite samples for A- mechanical testing and for B- *in vitro* bioactivity and bio-degradation studies

3.2.3.5 IN-VITRO BIO-COMPATIBILITY TESTS:

3.2.3.5.1 Hemo-compatibility test:

A standard hemolysis test was done using the protocol followed previously[73]. Briefly fresh goat blood was purchased from slaughter house in heparinized vials. 10mg of all samples (organo-apatites and HAP as control) were normalized in physiological saline for 30 minutes at 37°C. The anti-coagulated goat blood was diluted by sterilized physiological saline in the ratio of 5:4. To each normalized samples 0.5 ml of diluted blood was added and incubated for 60 minutes at 37°C. The negative control used here was 0.5mL of sterilized physiological saline, and the positive control was 0.5mL of 0.01N HCl. Thereafter, each tube was centrifuged, and then the absorbance of the supernatant was measured at 545 nm. The hemolysis percentage (Z) was calculated using the following formula:

$$Z\% = (D_t - D_{nc}) / (D_{pc} - D_{nc}) * 100$$

where D_t , D_{pc} , D_{nc} are absorbance of test, positive control and negative control at 545nm.

3.2.3.5.2 *In vitro* Bio-activity assessment:

The bioactivity is assessed by soaking the pressed organo-apatite pellet for 14 days in simulated body fluid (SBF) at 37°C. The ionic concentration of the SBF is similar to that of the ion concentration of human plasma. The bone bonding capacity of a material is assessed by its ability to form an apatite (carbonated hydroxyapatite) layer on its surface when kept in simulated body fluid.

The SBF was prepared based on a previously mentioned protocol [74], and the components were added in the following order:

Table – 3.3: *Composition of Simulated Body Fluid*

Order	Ingredient	Amount (g/L)
1	NaCl	6.547
2	NaHCO ₃	2.268
3	KCl	0.373
4	Na ₂ HPO ₄ .2H ₂ O	0.178

5	MgCl ₂ .6 H ₂ O	0.305
6	12 mL of 1M HCl	
7	CaCl ₂ . .2H ₂ O	0.368
8	Na ₂ SO ₄	0.071
9	Tris	6.057

The pH was adjusted to 7.4 with 1M HCl. Each pellet was soaked in SBF for a period of 14 days and after which the pellet was washed with distilled water and the feasibility of the apatite layer formed i.e. carbonated hydroxyapatite layer formed is detected through FTIR [75].

3.2.3.5.3 *In vitro* Bio-degradation study:

In-vitro biodegradation study of the pressed organo-apatite samples each roughly weighing 0.6g (dimension of 11-12mm in diameter and 3-4mm in height) was performed by soaking them in PBS containing 500 µg/ml of lysozyme. The composition of PBS (Phosphate Buffered Saline) is as follows:

Table – 3.4: *Composition of Phosphate Buffered Saline*

Ingredient	Amount (g/L)
NaCl	8
KCl	0.2
Na ₂ HPO ₄	1.44
KH ₂ PO ₄	0.24

The pH was adjusted to 7.4. The initial dry weight of the pellet samples were noted as W_I . The pellet samples were removed at regular time intervals and dried. W_F was calculated which is the final weight of the dried pellet. The weight lost % (W_R) was determined according to the formula given below [76]. The experiment was carried out in triplicates.

$$W_R = 100 - ((W_I - W_F)/W_I) * 100$$

A graph between the % weight lost and the time interval is plotted to monitor the degradation rate of the pellet.

3.2.4 *IN VITRO* CELL STUDY

3.2.4.1 CELL PROLIFERATION ASSAY:

Adipose Derived Stem cells (HiMedia, India) were used for bio-compatibility studies. The cells were cultured in low glucose Dulbecco's Modified Eagle's medium supplemented with 10% Fetal bovine serum (FBS) with 100U/ml penicillin, 0.1mg/ml streptomycin and 0.25 μ g/ml amphotericin-B. The *in vitro* cellular proliferation is assessed using MTT with or without keratin samples in 96 well plates under humidified condition in 5% CO₂ atmosphere at 37°C. 100 μ g/well of keratin extracted by the two different methods was added and the *in vitro* proliferation was checked for 3, 5 and 7 days. For organo-apatites and hydroxyapatite as control, samples were supplemented in concentration of 0.5mg/mL along with complete media. Similarly the *in vitro* proliferation assay was checked for 3, 5 and 7 days. Prior to sample seeding, the keratin samples were filter sterilized using 0.2 μ m filter, whereas the organo-apatites and hydroxyapatites powders were sterilized with UV irradiation followed by 70% ethanol wash. The samples were normalized with PBS thrice and the samples were suspended in complete media at desired concentration. In 96 well plates the seeding concentration per well was 10⁴ cells.

3.2.4.2 CYTOSKELETAL ORGANIZATION:

In order to evaluate the cytoskeletal architecture i.e. the F-actin morphology which indirectly gives insight on the cell spreading, TRITC-Phalloidin (Invitrogen) was used. The cells were seeded in cover slips in six plates at the seeding density of 10⁵ cells/cover slip and the complete media supplemented with organo-apatite and hydroxyapatite (concentration of 0.5mg/mL). The cells were fixed with 4% paraformaldehyde after 48hours and permeabilized with 0.25% Triton-X100 in PBS for 10 minutes and subsequently washed thrice with PBS. The cells were stained with 10 μ M TRITC-Phalloidin for 10 minutes followed by counter staining with 300 μ M DAPI (Invitrogen) for 5 minutes. The cells were then visualized in Confocal Microscope (Leica, Germany) at an excitation/emission wavelength of 545nm/573nm for TRITC and 358/461nm.

3.2.4.3 OSTEOGENIC DIFFERENTIATION POTENTIAL ASSESSMENT:

The osteogenic differentiation was inducted using the following osteogenic media which contains 10mM β -glycerophosphate, 100nM Dexamethasone and 0.2mM Ascorbic. The

osteogenic media was prepared as 20X stock in 10mL of incomplete media with 0.612g β -glycerophosphate, 7mg Ascorbic acid and 4 μ L of 2.5mM Dexamethasone. The 20X stock was made 1X using complete media and the seeded wells were supplemented with 1X osteogenic media. The osteogenic media was changed every three days till 21 days.

3.2.4.3.1 Alkaline Phosphatase Assay:

The Alkaline phosphatase is a key early osteogenic marker. After osteogenic induction with osteogenic media supplemented with 0.5mg/mL of hydroxyapatite and organo-apatites were added to 96 well plates. The seeding concentration was 10^4 cells/well. The ALP assay was done at regular intervals of time of 7, 14 and 21 days. The cells were lysed with 0.05% Triton-X100 in PBS. The ALP activity was determined using Sigma FastTM ALP kit. 200 μ L of the reagent was added to each well incubated for 1.5 hours and the absorbance was taken at 405nm immediately in UV-Vis spectrophotometer. The ALP activity is assessed colorimetrically by the ability of ALPase present in cells to cleave pNPP to a yellow color p-Nitrophenol which has a λ_{\max} of 405nm. The intensity of the yellow color is directly proportional to the ALPase present. [77]

3.2.4.3.2 Alizarin Red Staining:

The alizarin red stain helps to stain the calcium deposit on the osteogenic differentiated cells. 40mM Alizarin Red stain (Sigma Aldrich) was prepared in distilled water and filter sterilized. At the end of 21 days after osteogenic induction supplemented with the organo-apatite and hydroxyapatite (control) the cells were fixed with 4% paraformaldehyde for 15 minutes and washed with PBS thrice. The cells were then stained with 40mM alizarin red for 20 minutes and washed with distilled water till the unbound dye is removed. The micrographs were taken in inverted phase contrast microscope. The alizarin red was then eluted from the samples with 10% acetic acid and incubated for 30 minutes at 37°C, followed by 15 minutes incubation at 85 °C. The elution was collected and the absorbance was measured at 405nm in UV-Vis spectrophotometer. [78]

3.2.4.3.2 Osteocalcin and Run-x2 Expression Assessment:

The cells were seeded in cover slips in six plates at the seeding density of 10^5 cells/cover slip and the complete media supplemented with organo-apatite and hydroxyapatite (concentration of

0.5mg/mL). The staining was done based on a previously followed protocol [79]. The cells were fixed with 4% paraformaldehyde after 48hours and permeabilized with 0.25% Triton-X100 in PBS for 10 minutes and subsequently washed thrice with PBS [80]. To the permeabilized cells, primary antibody against osteocalcin (a key late stage osteogenic marker) at a concentration of 10µg/mL Anti-mouse Osteocalcin (Abcam, AB 13418) and incubated for 30 minutes. The unbound antibodies were washed with PBS. The secondary anti body against anti-mouse Osteocalcin was added at 5µg/mL (Anti-mouse Goat IgG, Alexa Fluor 594, Abcam, AB 150116) and incubated for 30 minutes. The unbound antibodies were washed with PBS. Similarly for anti-mouse Runx2 (Abcam AB11479) 10µg/mL was added. The cells were then stained with 10µM AlexaFluor488-Phalloidin for 10 minutes followed by counter staining with 300 µM DAPI (Invitrogen) for 5 minutes. The cells were then visualized in Confocal Microscope (Leica, Germany) at an excitation/emission wavelength of 495nm/518nm for AlexaFluor 488 and 358/461nm for DAPI and 590/617nm for AlexaFluor594.

3.2.5 STATISTICAL ANALYSIS:

The statistical analysis of the obtained experimental data was done using one-way ANNOVA. The p values of ≤ 0.05 for the given data expressed as mean \pm standard deviation were considered statically significant.

4. RESULTS AND DISCUSSION

4.1 EFFECT OF EXTRACTION PROCEDURE ON KERATIN'S STABILITY:

4.1.1 Protein Yield Quantification and SDS-PAGE:

The protein yield was calculated based on the colorimetric method using Bradford's method. The protein yield obtained by the two methods (for triplicates) of extraction process is shown in Table-4.1:

Table – 4.1: Protein yield determined by Bradford's method

Method	Protein yield (mg/ml)
Shindai method	7.56 ± 0.907
Sodium sulfide method	12.19 ± 0.422

The yield of protein was relatively more by sodium sulfide method as compared to the Shindai method. The obtained fractions of keratin extract were resolved in 15% polyacrylamide gel which is shown in Figure 4.1.

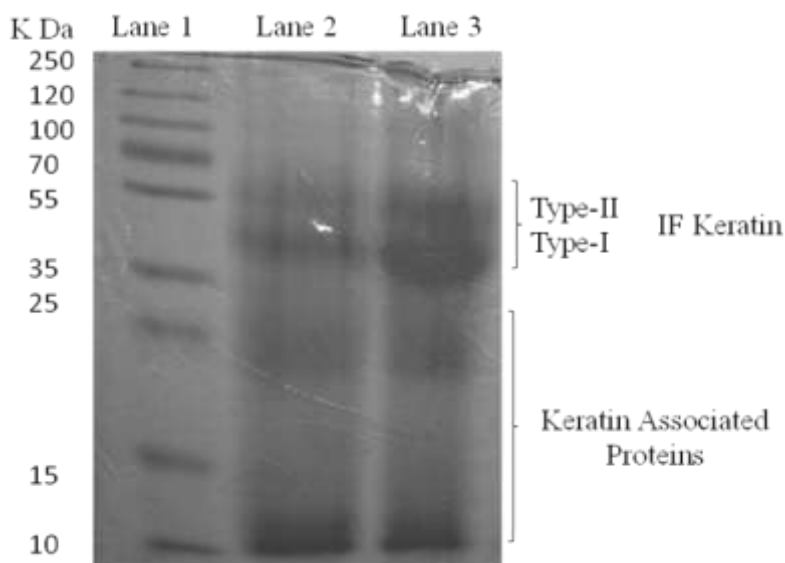


Figure - 4.1: SDS PAGE Pictogram; Lane-1 Molecular weight markers, Lane-2,3 Keratin isolated by Shindai method and Sodium Sulfide method respectively

In Shindai and Sodium sulfide method of extraction the keratin intermediate filament (IF) which consists of type-I and type-II keratin observed at about 40-60 kDa and the Keratin associated protein between 10-25 kDa, confirming that both the extraction protocols are successful in extracting keratin with varying degree of yield.

4.1.2 FTIR Analysis of extracted keratin:

The FTIR analysis of the keratin extracted by three different methods shows the presence of proteins which is inferred from the amide-I ($1600-1700\text{cm}^{-1}$) spectra and the amide-II spectra ($1500-1600\text{cm}^{-1}$). Figure-4.2 shows the FTIR spectra between $4000-400\text{cm}^{-1}$ of keratin extracted by the two methods.

The Amide I peak (*c* peak in Figure-4.2) which is in the range 1655 to 1650cm^{-1} , shows the C=N stretching. The Amide II peak (*b* peak in Figure-4.2) related to 1542 to 1520cm^{-1} , shows the N-H deformation and C-N stretching vibrations. These two peaks are characteristic of the keratin peaks found in literature as seen in Shuai Wang *et al.*, 2012; Andreia Vasconelos *et al.*, 2008; Jeanette M. Cardamone, 2010. [20, 81, 82] The peak (*a* peak in Figure-4.2) near 1045cm^{-1} suggests that there are C-O stretching vibrations found in aromatic and α -unsaturated chains, which are present in the polypeptide chain. The broad peak (*e* peak in Figure-4.2) between 2955 and 2854cm^{-1} represent the O-H stretching in the bound water molecules in proteins. The broad peak (*d* peak in Figure-4.2) near $3200-2900\text{cm}^{-1}$ represents the O-H, C-H, N-H stretching modes of the amino acids in the polypeptide chain. [82]

In order to investigate the percentage of secondary structures present in the extracted keratin and the effect of denaturants on the credibility of extraction procedure of keratin, the amide-I spectra between $1700-1600\text{cm}^{-1}$ was taken into consideration which hold the information. The amide-I spectra's absorbance in deconvoluted based on the conversion of the spectra to its second order derivative and the percentage of the area occupied by the deconvoluted curves to the whole area under the curve was estimated which gave the percentage of secondary structures present. [83].

From the Figures 4.3 and 4.4, the percentage of the secondary structures is estimated and it is evident that the sodium sulfide method is better method when compared to the Shindai method of extraction of keratin.

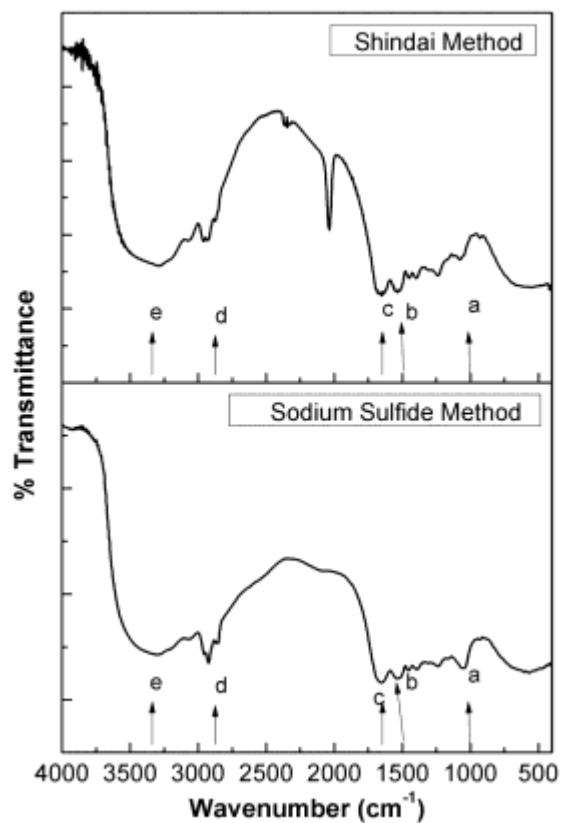


Figure – 4.2: FTIR Spectra between 4000-400 cm^{-1} of keratin extracted by Sodium Sulfide Method and Shindai Method

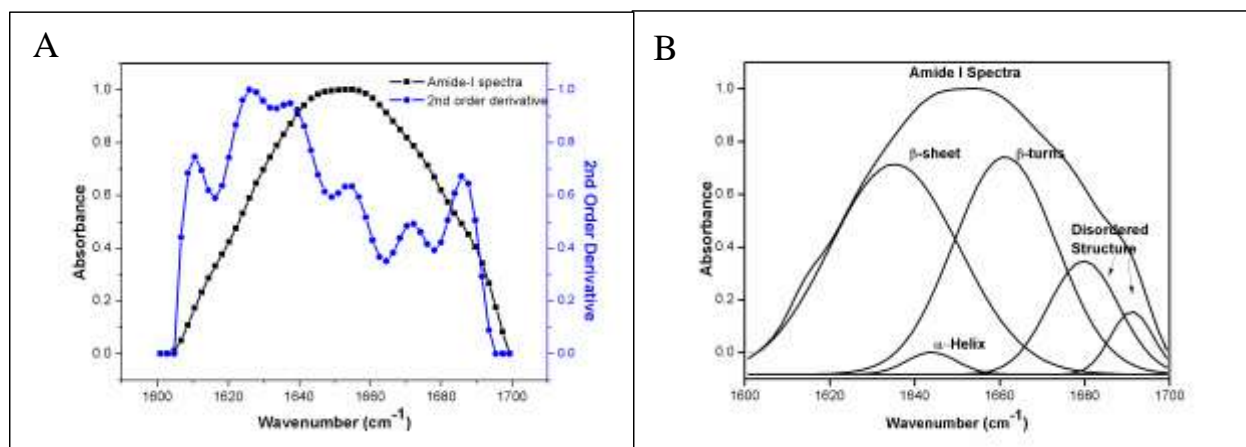


Figure – 4.3: Amide-I spectra and its 2nd order derivative; A) 2nd order derivative B) Deconvoluted Amide-I spectra for Keratin extracted by sodium sulfide method

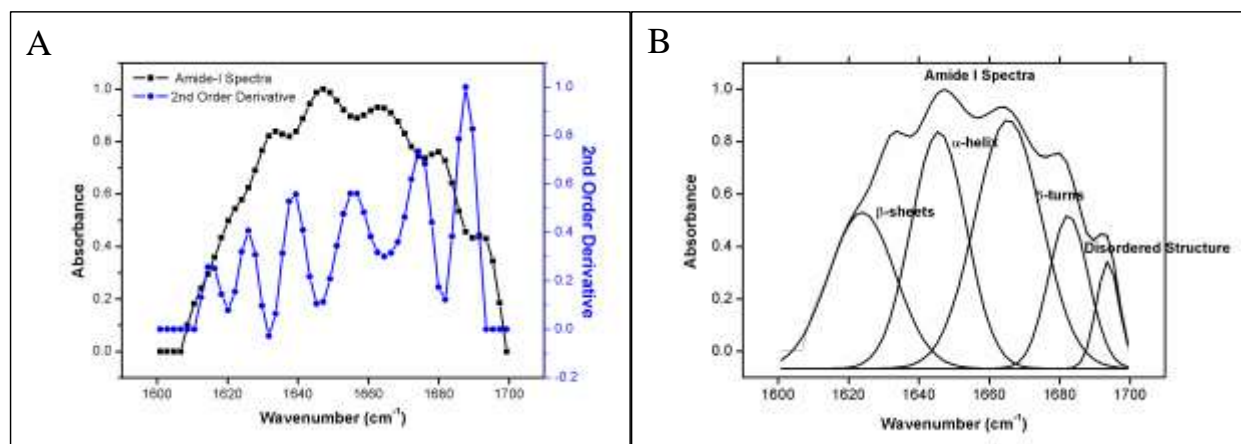


Figure – 4.4: Amide-I spectra and its 2nd order derivative; A) 2nd order derivative and B) Deconvoluted Amide-I spectra for Keratin extracted by Shindai method

Consequently when the denaturants are removed from the extraction buffer it must refold to its native conformation, but the tedious procedure applied by Shindai method makes the hard α -keratin extracted to lose its α -helical conformation. This may be due to the strain [84] undergoing due to the effect of many chaotropic agents used in the process of extraction such as urea, thiourea and DTT. The Table-4.2 summarizes the percentage of secondary structures present in keratin fraction extracted by the two methods.

Table – 4.2: Percentage of secondary structures obtained from deconvoluted Amide-I spectra

Secondary Structures	Percentage (Based on area under curve of deconvoluted spectra)	
	Sodium Sulfide Method	Shindai Method
β -sheet	25%	32%
α -helix	29%	8.6%
β -turns	27%	28.62%
Disordered structure	17%	9.96%

4.1.3 Circular Dichroism Spectroscopy Analysis:

The far-UV C.D spectra hold information regarding the secondary structures of the protein due to the presence of peptide bond, which absorbs below 240nm in the spectra. From the C.D spectra for the keratin obtained through sodium sulfide and Shindai method, the α -helical

conformation is lost (the positive maxima about 190nm, a decrease in intensity is noticed in case of Shindai method) which is in correspondence with the FTIR deconvolution results. Similarly there is an increase in β -sheet conformation noticed with keratin extracted through Shindai method.

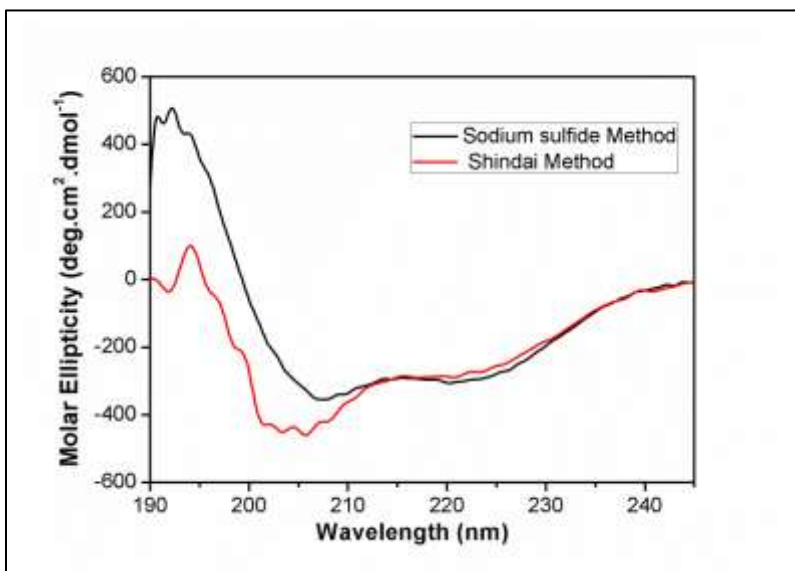


Figure – 4.5: Far UV Circular Dichroism Spectra of keratin extracted by sodium sulfide and Shindai method

The Table-4.3 depicts the percentage of secondary structure quantified through far-UV circular dichroism spectra.

Table – 4.3: Percentage of secondary structures obtained from far-UV C.D. spectra

	Percentage of Secondary Structures Present	
	Sodium Sulfide Method	Shindai Method
β -sheet	25.3%	47.8%
α -helix	36.3%	8.9%
Disordered structures	3%	6.5
Turns	35.4%	36.8

Keratins are predominantly α -helical structures. The effect of extraction procedure on the protein conformation is evident from the FTIR and C.D results. The α -helical conformation is lost relatively in Shindai method, and the keratin extracted incline towards a β -sheet conformation, whereas in case of the sodium sulfide method, the α -helical structure is retained.

4.1.4 Particle size distribution and Zeta potential analysis:

The particle size distribution profile of the keratin extracted by the two methods is seen in figure- The analysis were done after the lyophilized powder were mixed and stay for 2 hours and in Millipore water, particles analyzed are the stable structures of keratin protein after they self-assemble into aggregates. [11, 85] The Zeta potential of these keratins is also listed below in Table-4.4 obtained by the two methods:

Table – 4.4: Zeta potential and average diameter of keratin aggregates obtained by different methods

	Zeta Potential (mV)	Average Diameter (nm)
Shindai Method	-29.8 ± 8.48	228.5
Sodium Sulfide Method	-32.5 ± 4.36	209.0

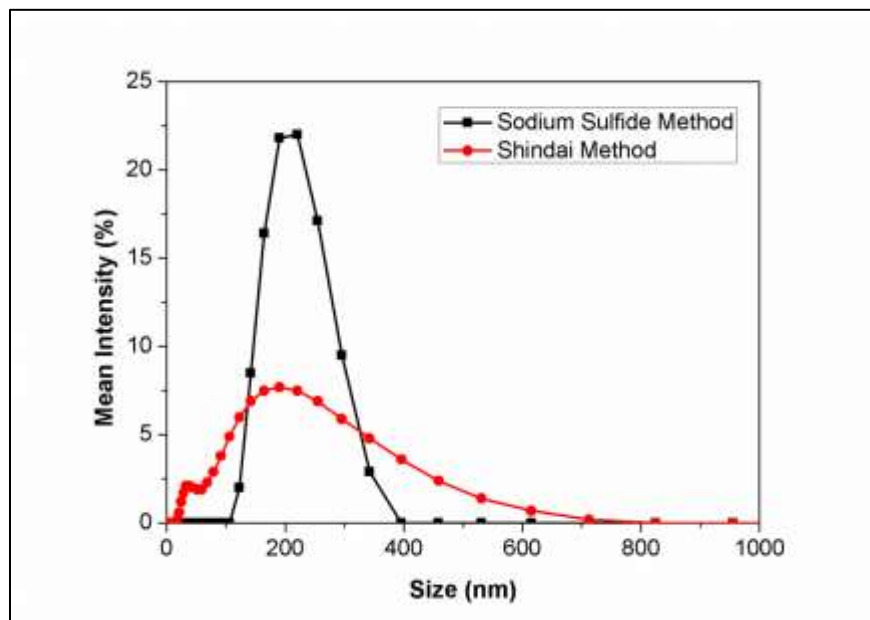


Figure – 4.6: Particle size distribution obtained by Dynamic light scattering

4.1.5. X-ray Diffraction analysis:

The small angle X-ray diffraction is widely used to study the structural transitions of biological macromolecules in solutions. From Figure-4.7, the s values corresponding to 0.008 \AA^{-1} , 0.011 \AA^{-1} , and 0.022 \AA^{-1} represent the α -helical conformation residing in intrinsically packed intermediate filament in keratins [86]. The intensity of the peaks decreased in the Shindai method and there is peak shift noticed for peak 0.0022 \AA^{-1} , suggesting a possible conformation change in the extracted keratin as observed from the Far-UV CD and FTIR spectra. Thus the Sodium sulfide method retains the α -helical conformation which is intrinsic to the intermediate filament domain regions of the α -keratin.

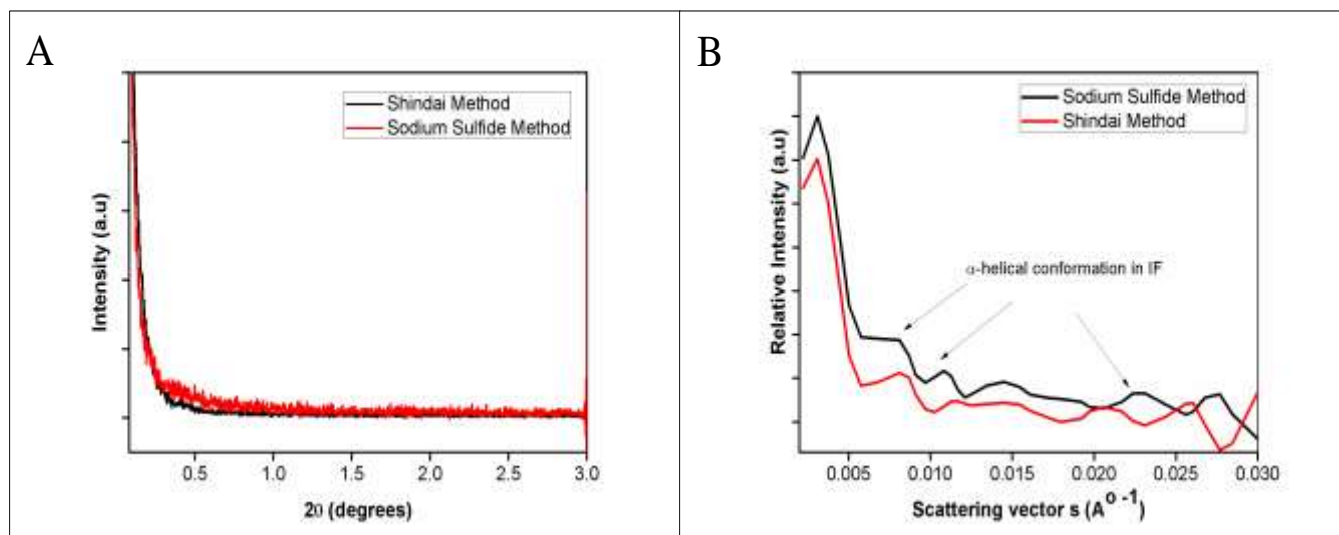


Figure – 4.7: A) Small angle x-ray diffractogram of Keratin extracted by Shindai and Sodium sulfide methods; B) Intensity vs. scattering vector plot from SAXS diffractograms of keratins extracted by Shindai and sodium sulfide method

The wide angle X-ray diffraction analysis of the keratin extracted by the sodium sulfide method reveals two amorphous peaks around 9.5° (peak a) and at 20.5° (peak b) as seen in figure-4.8. The peak at 9.5° corresponds to the α -helix and β -sheet conformation while the peak at 20.5° corresponds exclusively due to the presence of β -sheet conformation in the protein. [87, 88]. It is inferred from the Figure-4.8, that sodium sulfide retains the α -helical structure when compared to the Shindai method while the Shindai method relatively has more β -sheet conformation.

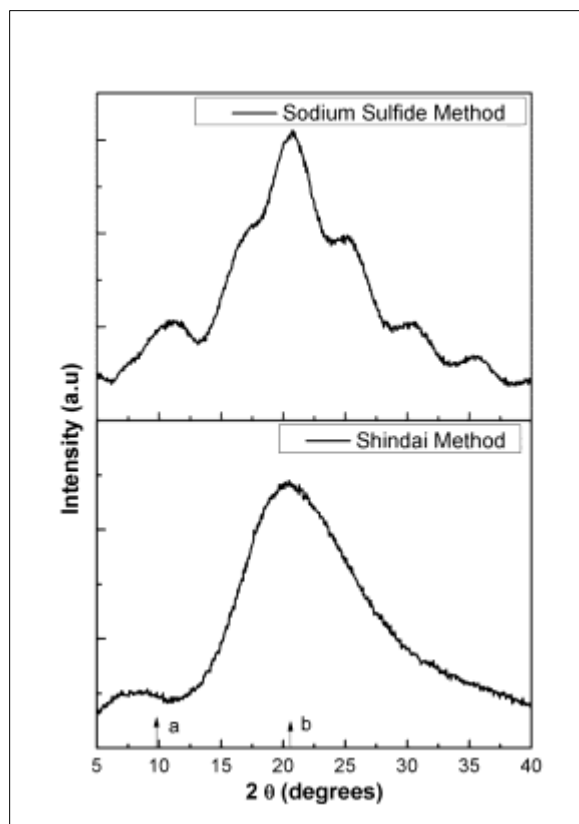


Figure – 4.8: Wide angle X-ray diffractogram of Keratin

4.1.6. *In vitro* Cellular Proliferation Assay:

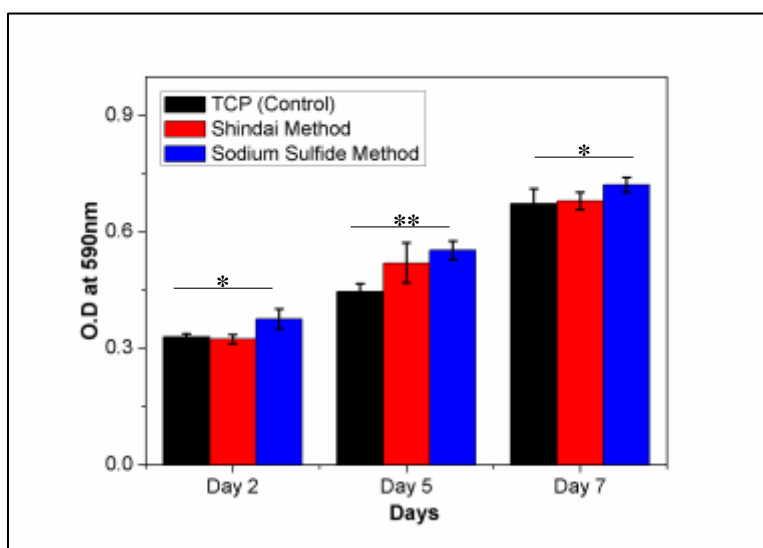


Figure – 4.9: *In vitro* Cellular Proliferation Assay through MTT assay; each point represents the mean \pm SD ($n=3$), * and ** represents significant difference between the population mean at $p>0.05$ and $p<0.05$ respectively

From Figure-4.9 the effect of soluble keratin (100 μ g/well) carried out in 96 well-plate over a period of 7 days was assessed for its cellular proliferation through MTT assay. It was found that keratin helped in cellular proliferation, the keratin extracted through sodium sulfide method was found to be better than the Shindai method. Keratin obtained through Shindai method, precipitated by trichloro-acetic acid on to culture ware dishes helped in better cellular adhesion and proliferation of 12 different cell lines such as HaCaT (keratinocyte cell line), HCK (Human Corneal Keratinocyte cell line), HCE-T (Human Corneal Epithelial Cell line) etc [4]. The keratin obtained through sodium sulfide method was also found to be bio-compatible and helped in cellular proliferation of L929 (fibroblast cell line) over a period of 12 days, and it was reported that keratin hydrogels were more conducive to fibroblast growth than collagen hydrogels [20]. Though there has not been any study comparing the keratins obtained through these two methods, this study throws insight of how α -keratin which retained its secondary conformations obtained through sodium sulfide method is relatively better than Shindai method in aiding cellular proliferation.

4.1.7 Cytoskeletal Organization:

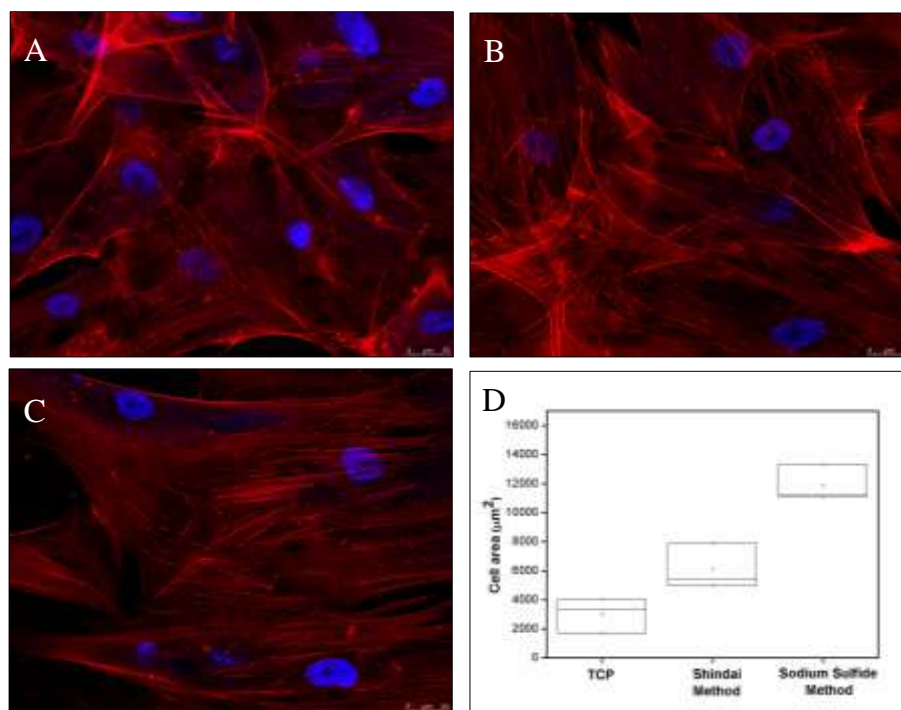


Figure – 4.10: Cytoskeletal organization A) Tissue Culture Plate B) Shindai Method and C) Sodium Sulfide Method D) Box plot showing cell area indicating cell spreadability

It was observed that with sodium sulfide method, the cell spreading was relatively better when compared to Shindai method and Tissue Culture Plate control. Keratin is known to contain cell adhesion motifs such as RGD (arginine-glycine-aspartate) and LDV (leucine-aspartate-valine) [16] and EDS (glutamate-aspartate-serine) to which $\alpha 5$, $\alpha 4$ integrin receptor family binds and hence enhancing its cell adhesion properties [17, 18]. The keratin based films [4] and sponges [89] are known for its ability to support cell adhesion and spreading, a report on use of bovine hoof derived keratin supplemented in media was also helpful in cell attachment and growth of 3T3-Li fibroblast cells when compared to untreated cells [90]. Through sodium sulfide method the structural integrity is retained which is much helpful in cell adhesion and spreading when compared to Shindai method.

4.1.8 Conclusion:

In conclusion, the keratin extracted by sodium sulfide method yield a relatively stable form of keratin which is inferred from the FTIR analysis, X-ray diffraction studies and Zeta potential assessments. In addition to the stability of the obtained keratin based on the protein yield, protein stability (where most of the secondary structures are stable and retained native to the α -keratin conformation) and also ease of extraction, the sodium sulfide method seems to be a better method for extraction of keratin from human hair. Keratin due to its biocompatible property due to its wound healing [21] and its ability to enhance cellular attachment and proliferation because of the presence of key cellular binding motifs such as RGD, LDV [18] are favorable for the development of biomaterials towards tissue engineering and the medical applications. The sodium sulfide method is relatively easier and less toxic method since the denaturant content used is comparatively less and can be easily removed by dialysis. Thus keratin extracted through sodium sulfide method (since the structural integrity of the α -keratin is retained much better) is used for the synthesis of organo-apatite for developing bone-biomimetic biomaterials.

4.2 SYNTHESIS AND CHARACTERIZATION OF KERATIN BASED ORGANO-APATITES:

The keratin based organoapatites were synthesized based on the concentration of keratin as seen in Table-4.5. The synthesized keratin based organoapatites had a slightly greyish white appearance as seen in Figure-4.11. The organoapatites were characterized further to know about its physical and chemical properties.

Table – 4.5: Concentration of Keratin added for organo-apatite synthesis

S. No.	Protein added in 0.06M H ₃ PO ₄	Composite denomination
1.	2.50 g/L	HAP-K50
2.	3.75 g/L	HAP-K75
3.	5.00 g/L	HAP-K100
4.	6.25 g/L	HAP-K125
5.	7.50 g/L	HAP-K150

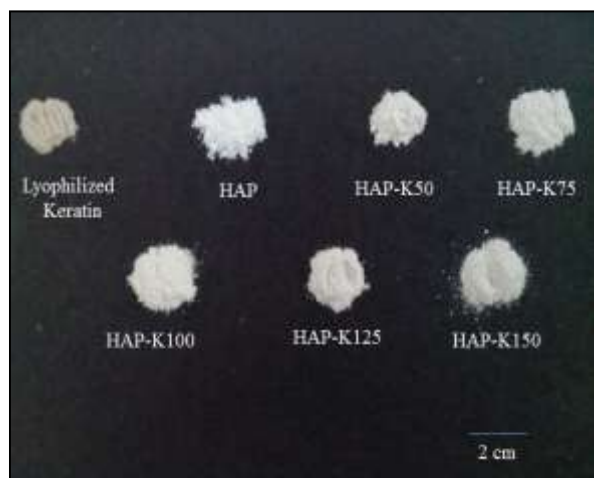


Figure – 4.11: Synthesized Keratin based Organoapatites showing greyish white appearance

4.2.1 Phase Analysis of synthesized organo-apatite:

As seen in XRD images (Figure-4.12), the hydroxyapatite was present in all the composites with its characteristic peaks at $2\theta = 25.88^\circ$, 28.16° , 31.97° , 32.96° , 34.11° [91]. The peaks were matched with JCPDS-84-1998 with a similarity score of 84 and no other calcium phosphate contaminants were noticed. Since the synthesis of apatite was done in low temperature to aid bio-mimetic apatite deposition along the keratin supramolecular network, the hydroxyapatite synthesized was amorphous in nature.

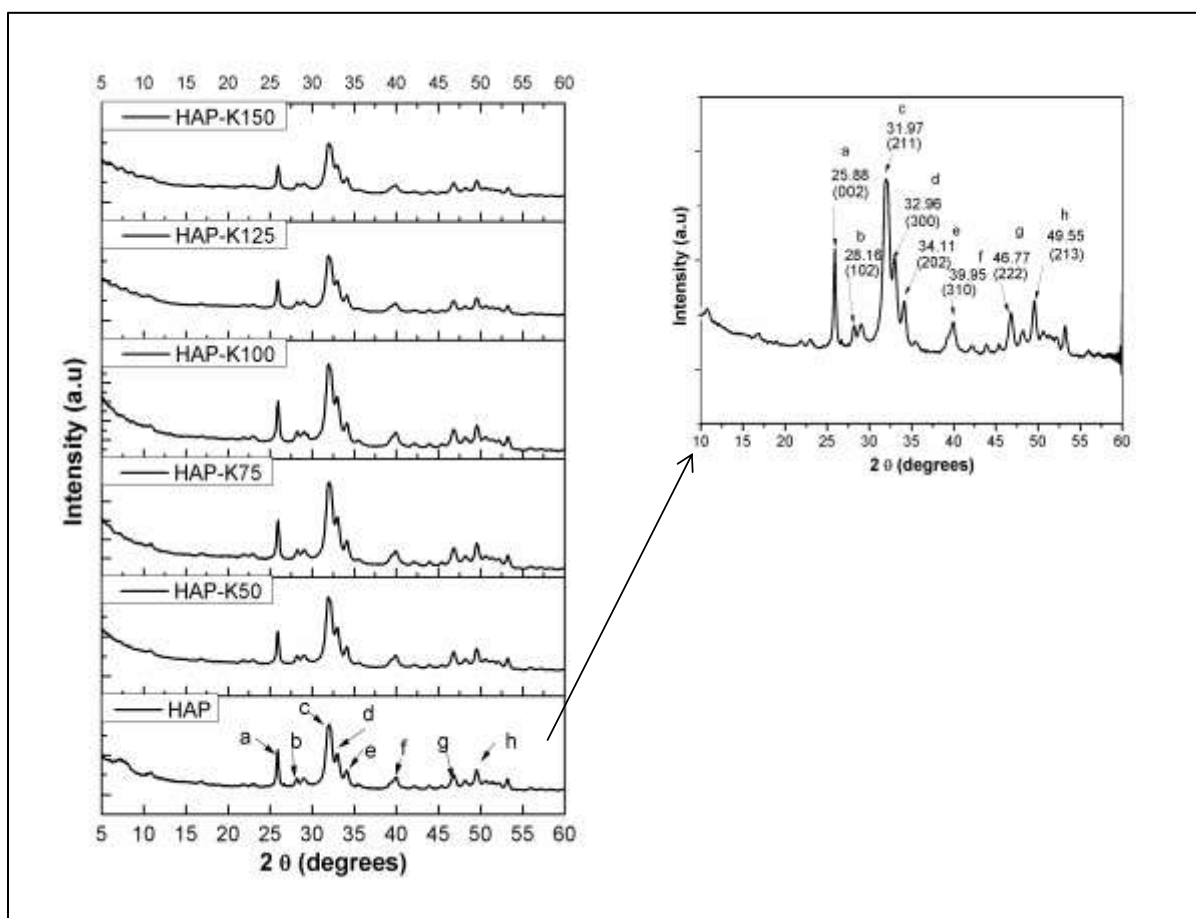


Figure – 4.12: X-ray diffractogram of hydroxyapatite and keratin based organoapatites; The HAP was matched with the JCPDS-84-1998 card with similarity score of 84

The percent crystallinity for the peak corresponding to the miller indices 211/300 helps to ascertain the amount crystallinity of apatite present in the composites. The crystallite size along the c-axis for the miller index (002) $2\theta = 25.88^\circ$ which gives the length of the crystal of hydroxyapatite formed. [92] The percent crystallinity and crystallite size were calculated and is

listed below in Table-4.6. It is observed that with increase in protein concentration the composites became more amorphous which is evident with the decrease in Crystallinity index.

Table – 4.6: *Percent Crystallinity and Crystallite size in 002 plane for different organo-apatites*

S. No.	Sample	Percent Crystallinity (%)	Crystallite size (nm)
1.	HAP	16.79	28.02
2.	HAP-K50	12.57	25.24
3.	HAP-K75	10.53	23.49
4.	HAP-K100	09.35	23.09
5.	HAP-K125	08.67	23.39
6.	HAP-K150	06.52	22.02

The nature of hydroxyapatite formed is generally amorphous under such ambient environment of temperature 40°C and pH 10-11. It is also seen in other organoapatites where directed growth of apatites in polymer network resulted in regulation of crystallite size as in the case of bi-template silk-fibroin/collagen [52] for hydroxyapatite synthesis and also in case of Bovine Serum Albumin (BSA) mediated synthesis [42], where the crystallite size decreased with increase in protein concentration. A similar observation was noticed in the keratin-based organo-apatite too, with increase in protein concentration the percent crystallinity decreased as well as the crystallite size indicating that keratin helps to regulate the size and formation of the hydroxyapatite formed along the protein fibril.

4.2.2 Morphological Study:

The morphological observation of the synthesized organo-apatites and pure hydroxyapatite as seen in Figure-4.13 revealed a rod shaped morphology. The size of the individual crystal was found to be in the range of 20-30nm with accordance to the XRD crystallite size measurement. It was observed that with increase in the protein concentration the size of the crystals decreased and became more compact suggesting that the keratin helped in regulating the size and distribution of the apatites along its supramolecular network. A similar observation of rod shaped crystals were also noticed in presence of bio-polymers such as collagen Type-I [44] and wool keratin [55] and synthetic polymer network of poly-vinyl alcohol [53].

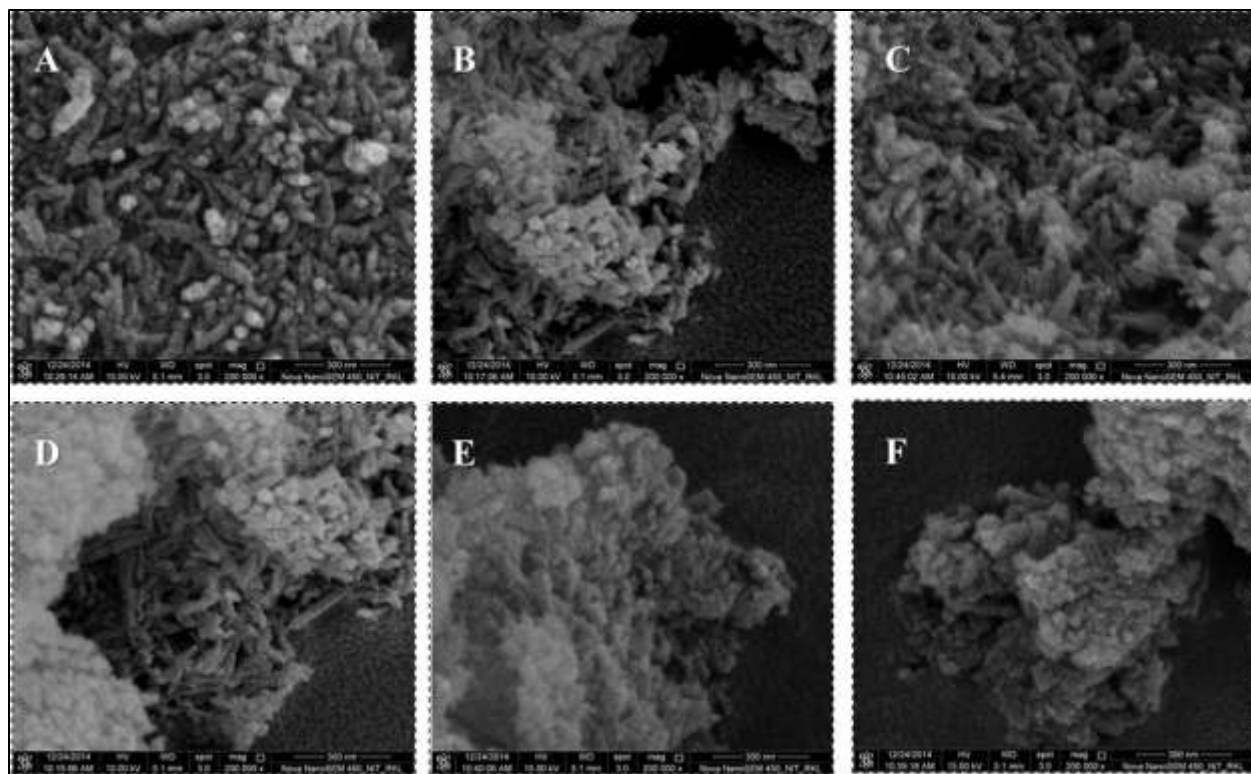


Figure – 4.13: FESEM Images of A) pure hydroxyapatite synthesized without protein and organo-apatite composites B) HAP-K50, C) HAP-K75, D) HAP-K100, E) HAP-K125 and F) HAP-K150

4.2.3 Functional Characterization:

4.2.3.1 FTIR Analysis:

From the FTIR spectra of keratin, the amide-II region corresponds to $(1500-1400\text{cm}^{-1})$ - C=N stretching and amide-I $(1700-1600\text{cm}^{-1})$ corresponds to N-H deformation and C-N stretching and OH stretching $(3200-2900\text{cm}^{-1})$ of bound water molecules [11, 82]. Similarly for pure hydroxyapatite, the degenerated bending mode $(400-560\text{cm}^{-1})$ ν_2 of O-P-O bonds of phosphate groups, the degenerated bending modes $(600-650\text{cm}^{-1})$ ν_4 of O-P-O bonds of phosphate groups, the bending mode $(1470, 870-880\text{ cm}^{-1})$ of ν_3 or ν_4 modes of CO_3^{2-} and OH stretching $(3450-3572\text{ cm}^{-1})$ of bound water molecules was observed [74, 91]. In the organo-apatites it was noticed that all the characteristic bands corresponding to the amide-I and amide-II were present, but little shift is noticed in the amide and amid-II region $(1600-1500\text{ cm}^{-1})$ suggesting a possible interaction between the apatite crystals formed and the polymer network. A similar observation

was noticed in cases of bio-polymer based template synthesis of organo-apatites [3, 52]. It is also observed that the broad OH-stretching noticed in the keratin protein was preserved in all the organo-apatite composites suggesting the interaction between the hydroxyapatite and the keratin polymer network.

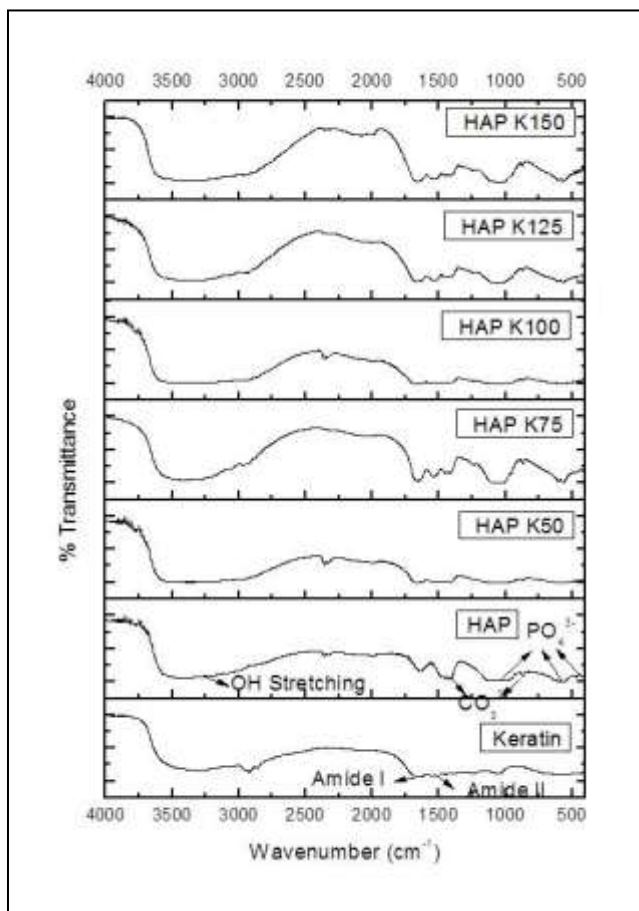


Figure – 4.14: FTIR spectra of keratin, pure hydroxyapatite and keratin based organo-apatite composites; a peak shift noticed in $1500-1700\text{cm}^{-1}$ suggesting possible interaction between the keratin and apatite crystals

In order to further investigate the interaction and the possible effect of apatite formation along the keratin fibril, the amide-I spectra which holds the information regarding the secondary structure of the protein is further investigated by taking the second order derivative of the amide-I spectra and fitting secondary sub-peaks as seen in Figure-4.15 and Figure-4.16 and assessing the deformation caused due to the apatite deposition along the keratin bio-polymer network.

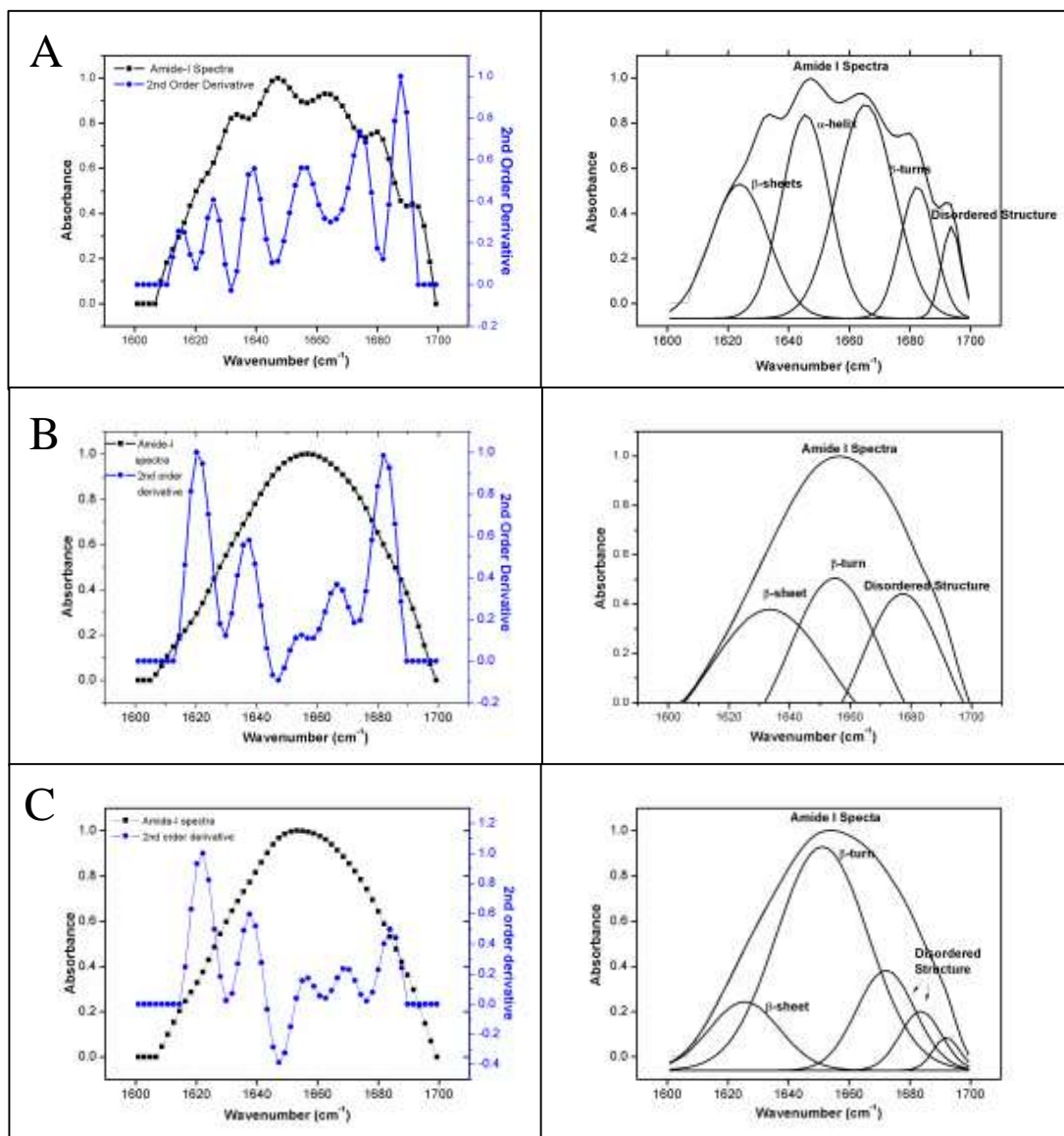


Figure – 4.15: Amide-I spectra and its 2nd order derivative and corresponding Deconvoluted Amide-I spectra for A) Keratin protein B) HAP-K50 C) HAP-K75

The keratin extracted through sodium sulfide method which was found to conserve the structural integrity of the keratin by maintaining its α -helical conformation was used for the synthesis of organo-apatite. When a supramolecular network of bio-polymers such as proteins either fibrous as in collagen type-I [40, 48, 49], silk fibroin [52] or globular protein such as bovine serum albumin (BSA) [41, 42] for synthesis of biomimetic organo-apatites, the nucleation of the apatite is initiated at the COO^- ends of the amino-acid side chains to which calcium precursors bind and initiate the apatite formation. After initiation growth of the apatite crystal is regulated by the

availability of bio-polymer network and the concentration of the bio-polymer (keratin) in the media. It was observed that with the increase in protein concentration, the composites formed were oriented towards more and more having disordered structures and β -turns. The stable secondary structures of α -helix and β -sheet conformation were lost indicating the interaction of apatite crystals along the keratin fibril supramolecular network.

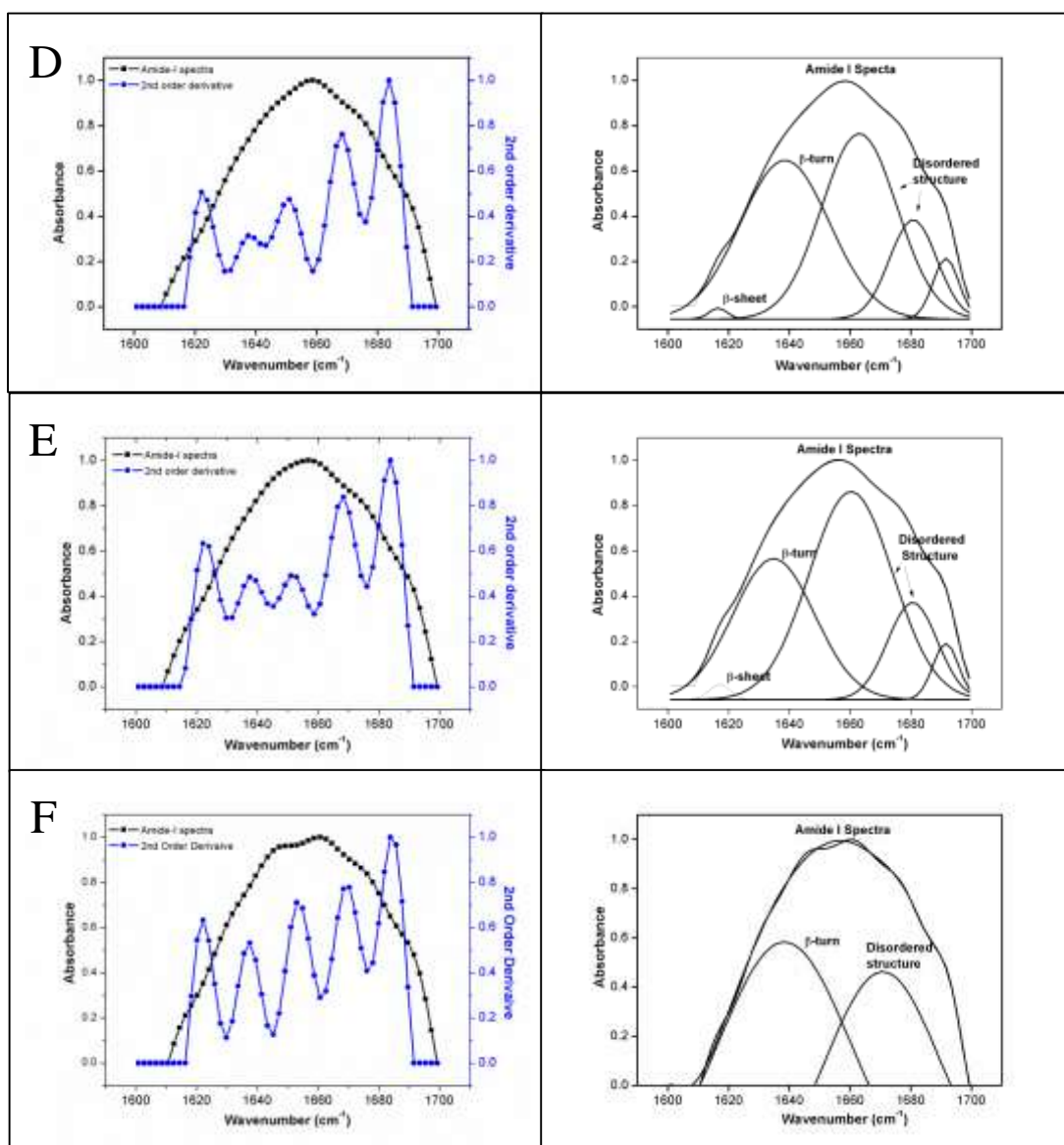


Figure – 4.16: Amide-I spectra and its 2nd order derivative and corresponding Deconvoluted Amide-I spectra for D) HAP-K100 B) HAP-K125 C) HAP-K150

Table-4.7 summarizes the percentage of secondary structures present in the composite, and it is evident that HAP-K150 has lost all its secondary conformation. The nucleation and growth

depends strictly upon the concentration of the polymer solution, and with more increase in protein concentration the growth and interaction is not regulated and may be heterogeneous nucleation and growth of apatite crystals resulted in such conformational changes. Till now there has not been any study carried out on the effect of apatite nucleation and growth on the protein's secondary structure.

Table – 4.7: Percentage of secondary structures obtained from deconvoluted Amide-I spectra

Secondary Structures	Percentage (Based on area under curve of deconvoluted spectra)					
	Keratin	HAP-K50	HAP-K75	HAP-K100	HAP-K125	HAP-K150
β -sheet	25%	31%	13%	7%	7%	--
α -helix	29%	--	--	--	--	--
β -turns	27%	35%	51%	34%	24%	60%
Disordered structure	17%	34%	28%	47%	58%	33%

4.2.3.2 C.D Analysis:

The Far-UV circular dichroism spectra help us to understand better the secondary structure conformation obtained by the keratin in the organo-apatite composites. From Figure-4.17 it is inferred that the β -sheet region in the organo-apatite are gradually unfolded, which is in correspondence with the results obtained through the deconvoluted FTIR spectra of amide-I region. The keratin in the composites gradually unfolds and shifts to a disordered structure, as the apatite synthesis occurs. In a similar observation, a denovo synthesized protein JAK-1, the hydroxyapatite helped to regulate its folding by interacting with the protein functional groups [93], suggesting the apatite formed has a role to play in the misfolding of the protein. It is seen in certain fibrous protein as in case of fibrin [94] and hard α -keratin [95] when it undergoes some stress, there is α -helix to β -sheet conformation. Similarly in the case of organo-apatite, the α -

helix to β -sheet or disordered structure transition may be due to the microscopic stress encountered while formation of hydroxyapatite along the keratin fibril.

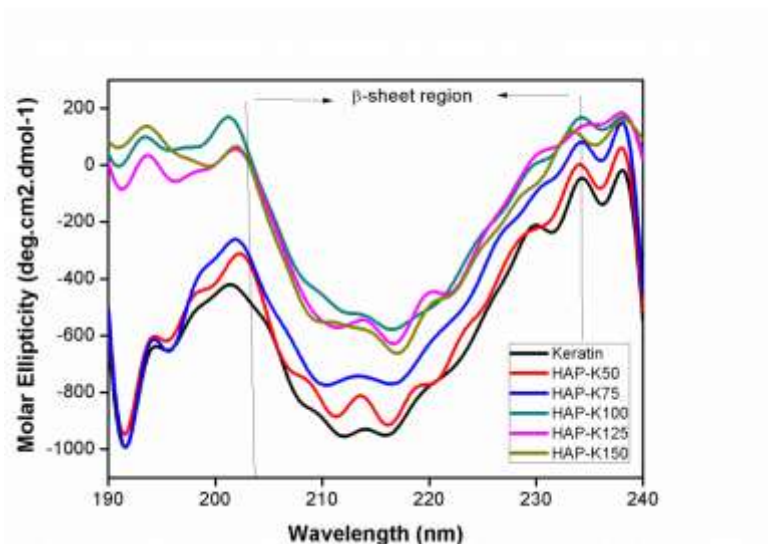


Figure – 4.17: Far-UV CD spectra of the organo-apatite composites

4.2.4 Thermal Analysis:

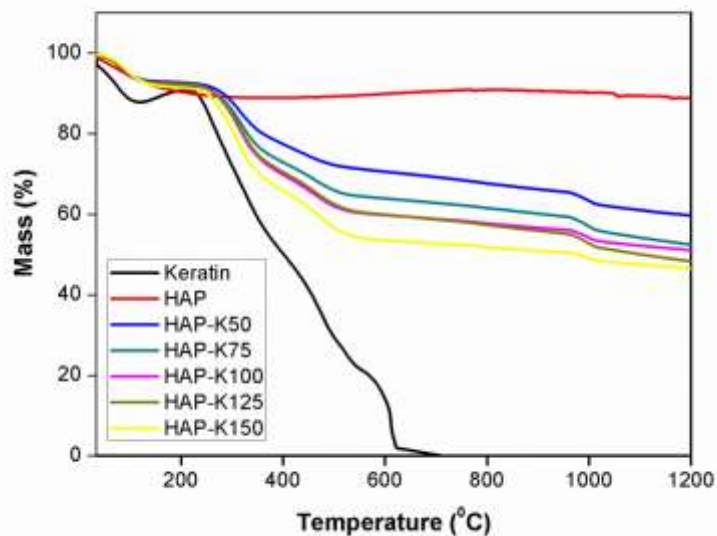


Figure – 4.18: TGA curve of keratin, pure hydroxyapatite and keratin based organo-apatite composites

From Figure-4.18, the thermo-gravimetric analysis (TGA) curve the initial weigh loss from 40 to 120°C is due to the evaporation of water from the composites. The keratin got combusted totally at about 620°C which is in correlation with previous studies [80, 90]. Therefore the region between 120-700°C is the region where all the organic matter in the composites are lost. Above 950°C there is dehydroxylation of hydroxyapatite and release of CO₂ which results in the weight loss of about 11% [96, 97]. From the TGA curve based on the elimination of organic content the percent of hydroxyapatite present can be calculated, which is listed below in Table-4.8:

Table – 4.8: *Percentage of hydroxyapatite present in the organo-apatite composites*

S.No.	Composite	Percent of HAP in Composite
1.	HAP-K50	76.69
2.	HAP-K75	69.72
3.	HAP-K100	65.56
4.	HAP-K125	63.88
5.	HAP-K150	58.09

Bone contains about 65-70% inorganic content which is the hydroxyapatite present in the mineralized collagen network [7, 98] and from the organo-apatites synthesized HAP-K100 and HAP-K125 are relatively close to the range of the bone mimetic inorganic phase content, while other composites contain relatively higher and lesser apatite content.

4.2.5. Mechanical Strength Testing:

The compressive strength of the synthesized organo-apatites was compressed into pellets by uniaxial compression. The pellets were subjected to compressive testing and the corresponding stress-strain curve is given in Figure-4.19. It is observed that the increase in organic content in the composites resulted in decreasing of the compressive strength and Young's modulus as shown in Table-4.9.

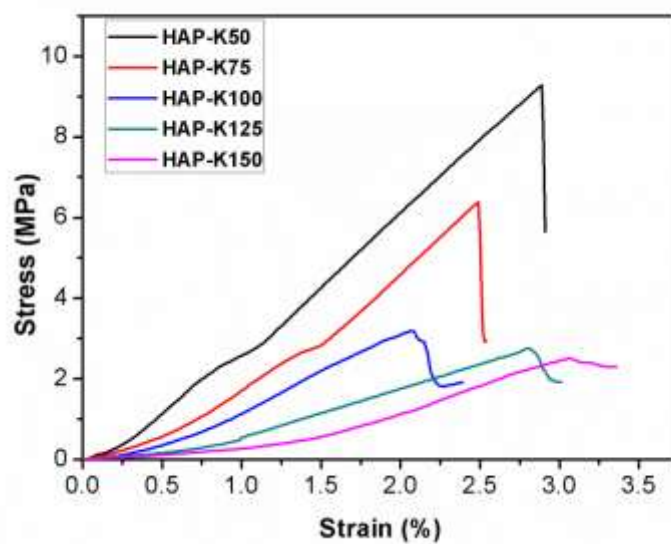


Figure – 4.19: Stress-strain curve for keratin based organo-apatites

Table – 4.9: Compressive strength and Young's modulus of keratin based organo-apatite

Samples	Max. Compressive Strength (MPa)	Young's Modulus (MPa)
HAP – K50	9.36 ± 0.12	3.66 ± 0.04
HAP-K75	6.395 ± 0.03	3.65 ± 0.05
HAP-K100	3.275 ± 0.07	2.02 ± 0.07
HAP-K125	2.735 ± 0.03	1.21 ± 0.06
HAP-K150	2.43 ± 0.08	1.3 ± 0.05

The porosity of the pellets also increased owing to the increase in the organic content present in the composites as seen in Table-4.10. The porosity was measured by a previously mentioned protocol [99] and the density of hydroxyapatite was taken as 3.16 g/cm^3 [99] and the density of human hair keratin was taken as 1.28 g/cm^3 [100], from which the densities of individual organo-apatite composites were calculated as listed in Table-13. The protein counterpart present in the organo-apatite is the region where micro-pores are developed which resulted in a porous structure of the compressed pellet. A similar observation was also noticed in case of collagen-

hydroxyapatite composites [3, 99] which were compressed by cold isostatic pressure (CIP), and with increase in collagen content the compressive strength decreased in the compressed pellet.

Table – 4.10: Percent porosity of the organo-apatite uniaxially compressed pellets

Samples	Radius (mm)	Height (mm)	Volume (cm ³)	Mass (g)	ρ	ρ	Porosity (%)
					(scaffold) (g/cm ³)	(material) (g/cm ³)	
K50	5.835	5.65	0.604032	0.97	1.605875	2.503	37.827 ± 2.81
	5.475	7.01	0.659805	0.994	1.506506		
K75	5.565	7.06	0.686538	0.96	1.39832	2.37	41.245 ± 0.34
	5.49	7.62	0.721156	1	1.386663		
K100	5.52	7.14	0.683134	0.985	1.441884	2.46	41.686 ± 0.42
	5.605	6.89	0.679673	0.97	1.427157		
K125	5.89	5.48	0.596954	0.94	1.574661	2.728	41.911 ± 0.52
	5.735	5.89	0.608292	0.97	1.59463		
K150	5.69	6.41	0.651647	0.98	1.503882	2.596	43.106 ± 1.47
	5.32	7.76	0.689628	1	1.450058		

4.2.6 *In vitro* Bio-compatibility study

4.2.6.1 Hemo-compatibility:

The hemo-compatibility test was done using goat blood obtained from the local slaughter house. It was found that all the organo-apatites were found to be non-hemolytic as seen in Table-4.11. It is reported that when the percent hemolysis (Z) is greater than 5, the material is hemolytic, while 2-5 is slightly hemolytic and lesser than 2 is non-hemolytic[73]. Keratiene (reduced form of keratin) used in the study as a template for the development of organo-apatites, is known to a known hemo-stat and used in blood clotting applications [101, 102], therefore the hemo-compatibility test of the synthesized keratin based organo-apatites were performed. It was found all the composites were non-hemolytic and hence can be used for bone tissue engineering applications.

Table – 4.11: Percent hemolysis of the hydroxyapatite and keratin based organo-apatites

S. No.	Sample	O.D at 545nm				Percent Hemolysis	
		R1	R2	R3	Mean	(Z)	
1	HAP	0.053	0.051	0.053	0.052333	0	
2	HAP-K50	0.054	0.051	0.055	0.053333	0	
3	HAP-K75	0.06	0.051	0.052	0.054333	0	
4	HAP-K100	0.06	0.05	0.056	0.055333	0	
5	HAP-K125	0.058	0.052	0.061	0.057	0	
6	HAP-K150	0.057	0.054	0.058	0.056333	0	
7	Positive Control				0.095		
8	Negative Control				0.06		

4.2.6.2 *In vitro* Bioactivity study

The ability of a material to form a layer of carbonated hydroxyapatite on its surface is a direct indication of the bone bonding ability, which is assessed by placing a bone conductive material in simulated body fluid for over a period of 14 – 21 days [103]. For carbonated hydroxyapatite characteristic peaks (as seen in Figure-4.20) in the region of 1032 cm^{-1} which corresponds to triply degenerated asymmetric stretching mode of phosphate group of P-O (peak a), in the region of 1110cm^{-1} due to the presence of CO_3^{2-} in non-stoichiometric apatites present in carbonated hydroxyapatites (peak b) and in region of 2000 cm^{-1} corresponding to harmonic overtone. [91] In order to determine the $r_{c/p}$ ratio which is a direct correlation of the bio-activity content (i.e. amount of carbonated apatite present), a previously published protocol was followed [75]. Briefly, the keratin spectra were negated from the organo-apatites samples by running a background of keratin and then the FTIR spectra of the organo-apatites were obtained. The $r_{c/p}$ ratio was calculated based on the formula:

$$r_{c/p} = \text{Area of } \text{CO}_3^{2-} \text{ peak} / \text{Area of } \text{PO}_4 \text{ peak}$$

The $r_{c/p}$ value is a direct indication of the amount of carbonate content present in sample, which in turn signifies the amount of apatite deposited on the material.

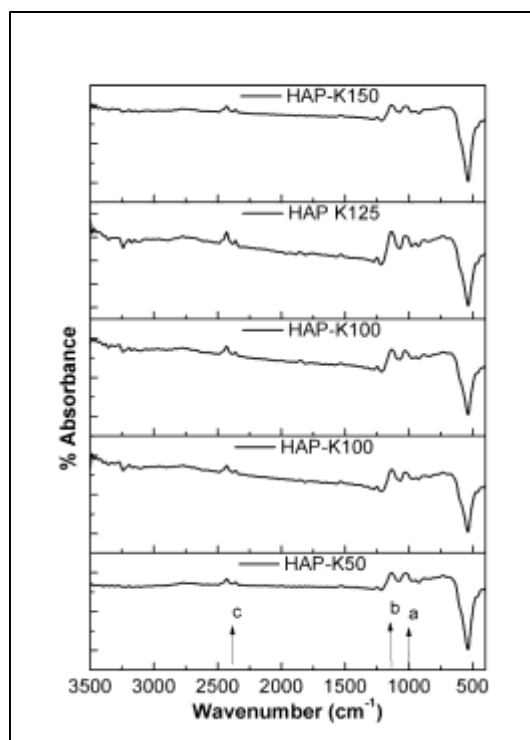


Figure – 4.20: FTIR Spectra of organo-apatites pellets after soaking in SBF for 14 days to assess the bio-activity

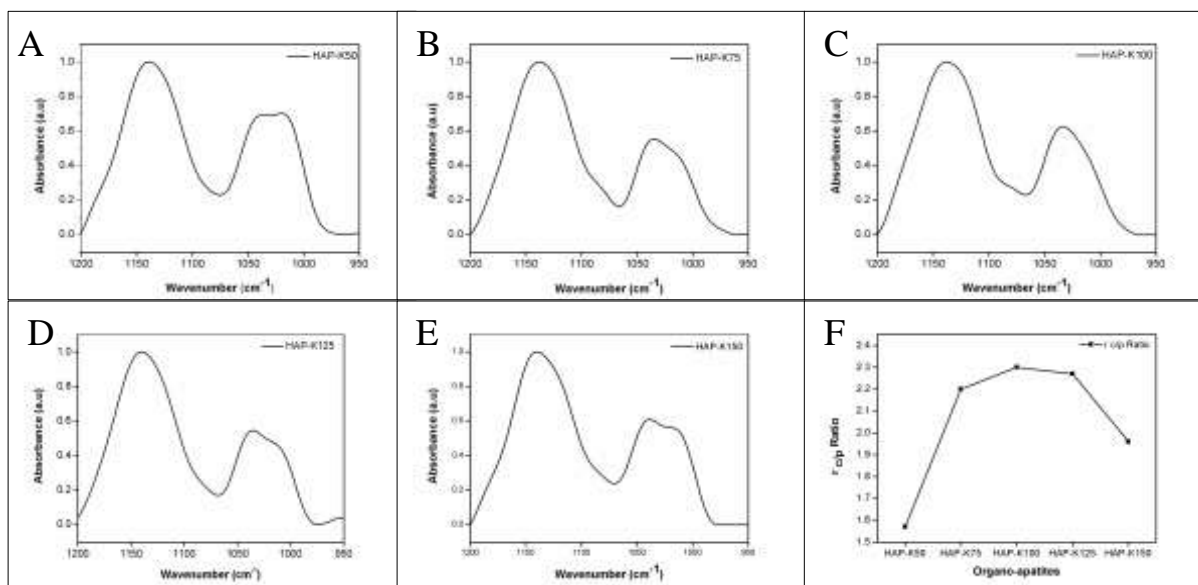


Figure – 4.21: FTIR spectra between $1200-950\text{cm}^{-1}$ corresponding to carbonate and phosphate groups; A) HAP-K50, B) HAP-K75, C) HAP-K100, D) HAP-K125, E) HAP-K150 and F) Bioactivity assessment through r_{cp} ratio

From Figure-4.21-F, it is found that the $r_{c/p}$ ratio increased with increase in organic content as found in HAP-K50, HAP-K75, and HAP-K100 and eventually decreased with HAP-K125 and HAP-K150. Thus the composite HAP-K100 was found to have the highest $r_{c/p}$ value, indicating that it is more bio-active than the other composites.

4.2.6.3 *In vitro* Bio-degradation study:

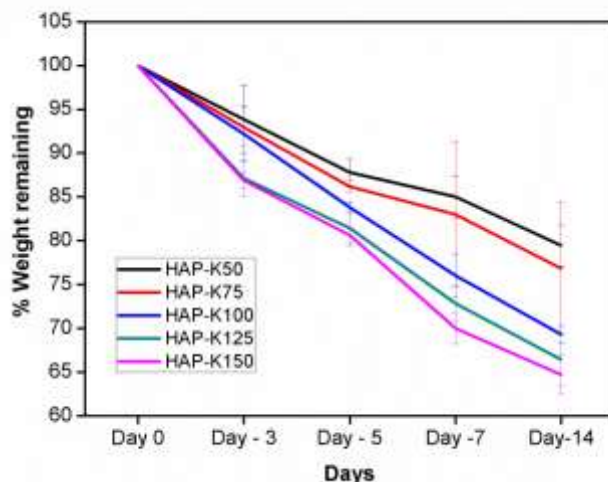


Figure – 4.22: Bio-degradation Study of organo-apatites

From Figure-4.22 it is inferred that with increase in organic content in the composites, the rate of degradation is more suggesting the protein counterpart helps to hold the composites as a binder, With due course in time the lysozymes cleaves the protein content in the composites and hence the composites degrade faster.

In conclusion, from the physico-chemical characterizations, it was observed that the protein concentration has a role to play in the heterogeneous nucleation and growth of the hydroxyapatite crystals along the keratin fibril. The percent crystallinity and crystallite size decreased with increase in protein content in the composites. The protein-apatite interaction was analyzed using FTIR analysis and it was found that there was gradual transition of the secondary structures to disordered structures. The HAP-K100 and HAP-K125 were found to be more bio-active than the other composites with a moderate degradability and a young's moduli of 2.02 ± 0.07 and 1.21 ± 0.06 MPa respectively which is relevant for application as bone fillers.

4.3 *IN-VITRO* CELL STUDY AND OSTEOGENIC DIFFERENTIATION POTENTIAL OF KERATIN BASED ORGANO-APATITES:

4.3.1 *In vitro* Cellular Proliferation by MTT Assay:

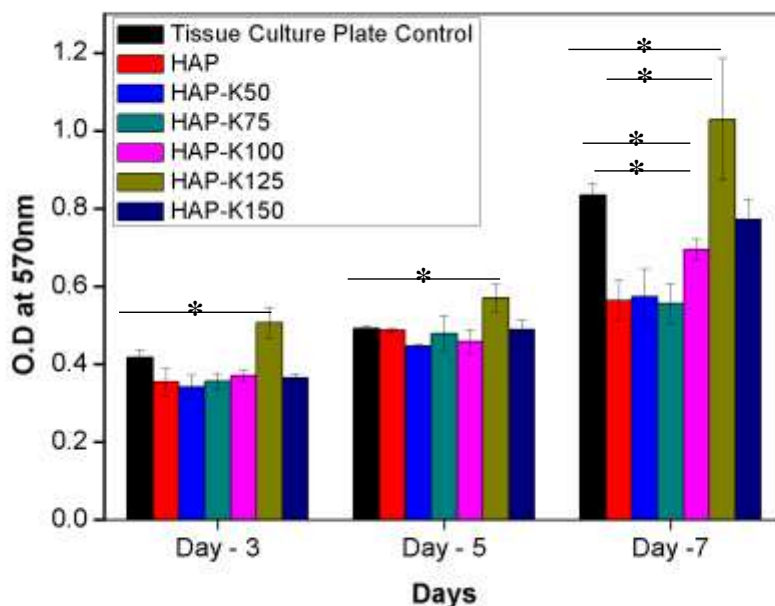


Figure – 4.23: *In vitro* cellular proliferation through MTT assay; each point represents the mean \pm SD ($n=3$), * represents significant difference between the population mean at $p < 0.05$

MTT (3-(4,5-dimethylthiazol-2-yl)-2,5-diphenyltetrazolium bromide) is a tetrazolium salt which is reduced by mitochondrial dehydrogenase enzyme to formazan crystal whose λ_{\max} is around 570nm. The intensity of purple formazan crystal is a direct indication of the live cells present whose ability to reduce the formazan crystal is assayed, which in directly gives the proliferation rate of cells in presence of the samples. From Figure-4.23 and Figure-4.24, it is seen that composites HAP-K100, HAP-K125 and HAP-K150 were showing better viability at the end of day-7. The composite HAP-K100 was shown to better than the control HAP and tissue culture plate control. The HAP-K100 is seen to be more bio-active and its organic:inorganic content is much similar to that of the bone, proving that they are helpful in inducing cellular proliferation. A similar observation is noted in case of wool keratin and collagen based composites, wherein when the composites' organic to inorganic ratio when it is similar to that of the bone it led better cellular proliferation. [3, 55, 56]

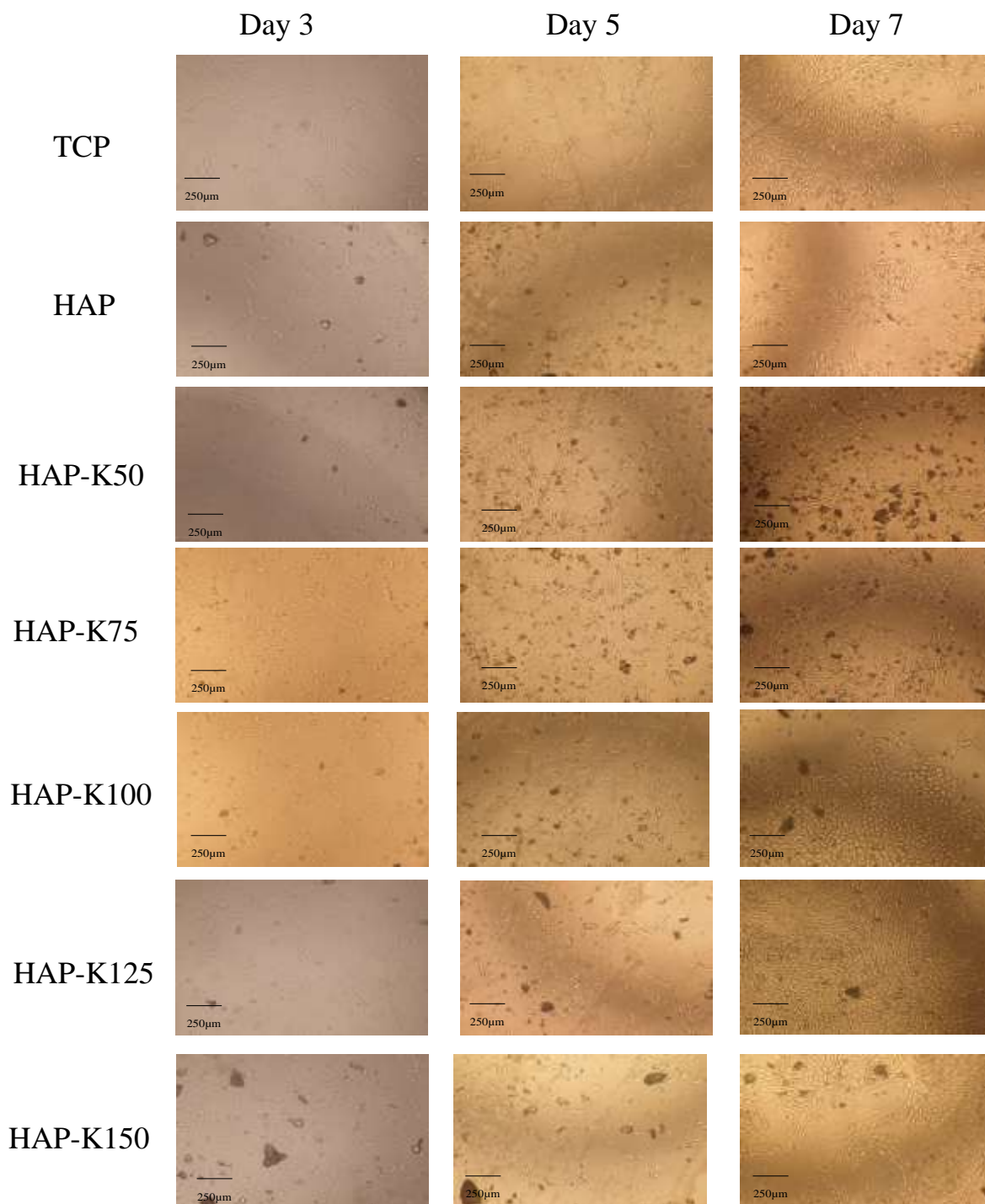


Figure – 4.24: Phase contrast microscopy images at different time intervals while assessing cellular proliferation of ADSCs in TCP (Tissue culture plate) as control and in presence of hydroxyapatite and keratin based organo-apatite composite

4.3.2 Cytoskeletal Organization:

The introduction of protein in apatite based composites has led to better cellular adhesion and cellular spreading as observed in previous study with fibrin [104], collagen [105, 106] and fibroin [107] through $\alpha 5\beta 1$ mediated integrin receptor binding crucial for cell adhesion and cytoskeletal organization [108]. It is observed from Figure-4.25 that in presence of HAP, the cell spreading is less when compared with other keratin-hydroxyapatite organo-apatite composites, indicating that the keratin plays a role in cell adhesion and cell spreading. Keratin possesses key amino acid motifs such as RGD (arginine-glycine-aspartate) and LDV (leucine-aspartate-valine) [16] and EDS (glutamate-aspartate-serine) to which $\alpha 5$, $\alpha 4$ integrin receptor family binds and hence enhancing its cell adhesion properties [17, 18]. The composites HAP-K100 and HAP-K125 are show more spreadability assessed by calculating the cell area occupied by the cell, indicating that the composites which are more mimetic to the bone helped in cell adhesion better than the other composites. A similar observation is noticed in Saos-2 (sarcoma osteogenic cell line) which showed better cell spreading with wool keratin-hydroxyapatite composite with a ratio of organics and inorganics similar to that of bone. [55]

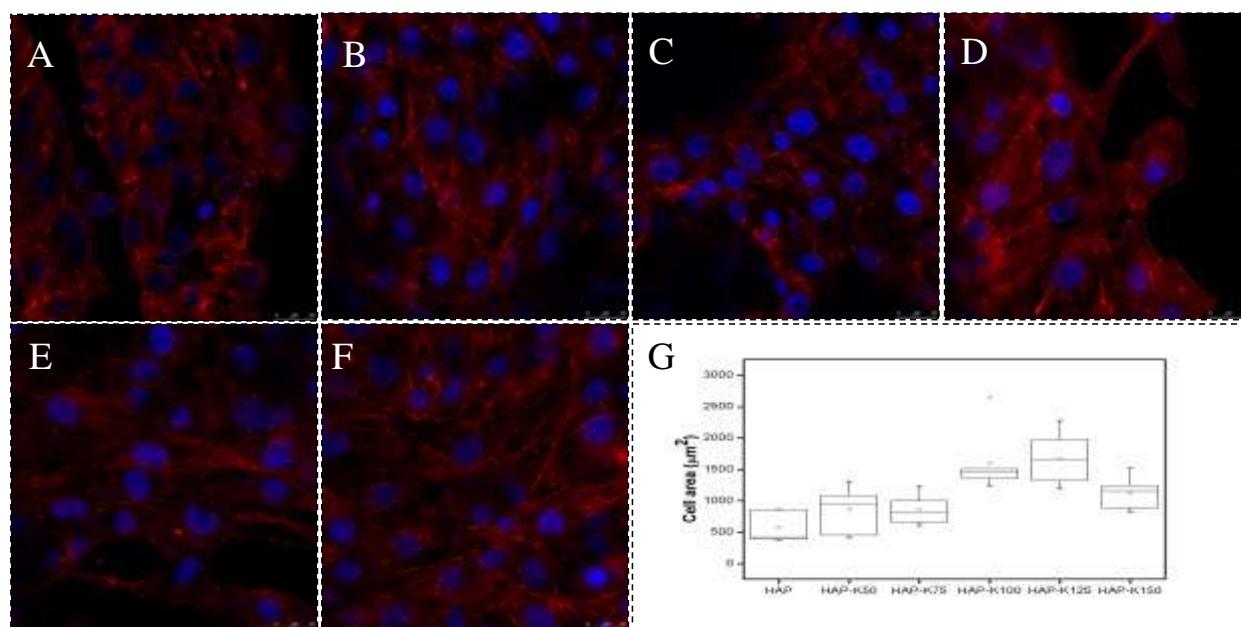
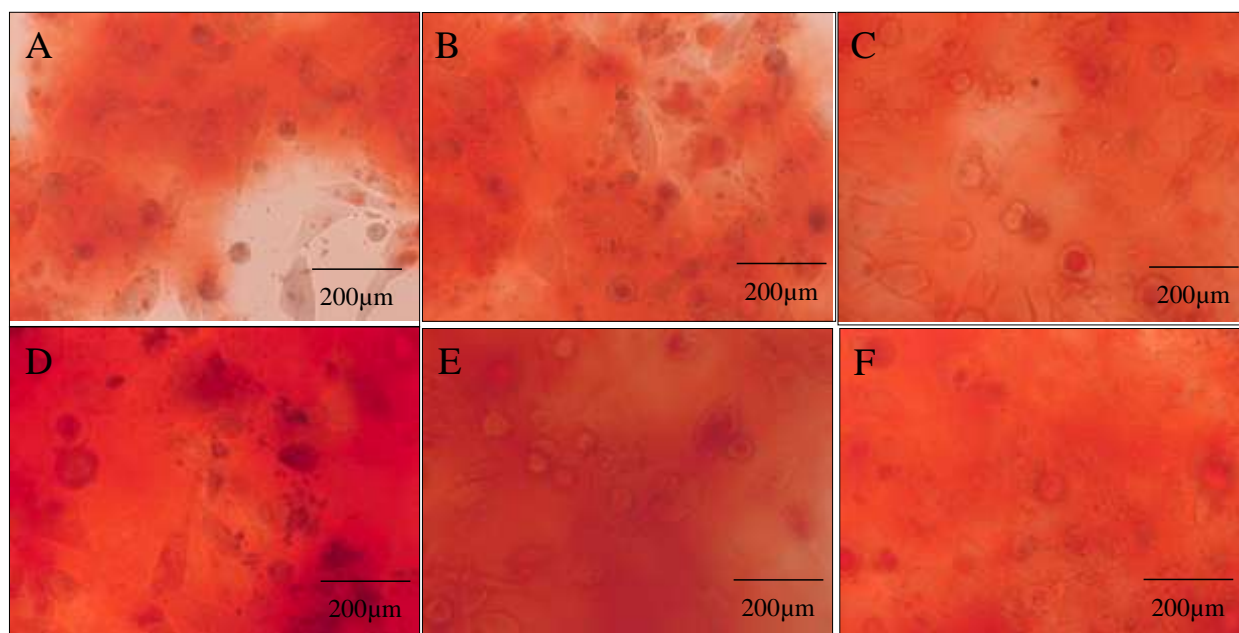


Figure – 4.25: Cytoskeletal organization in presence of hydroxyapatite and keratin based organo-apatites; A) HAP, B) HAP-K50, C) HAP-K75, D) HAP-K100, E) HAP-K125, F) HAP-K150 and G) Box plot showing cell area indicating cell spreadability

4.3.3 Osteogenic Differentiation Potential:

4.3.3.1 Alizarin red staining:

Mineralization of osteogenically differentiating cells can be assessed by use of Alizarin Red staining method. The alizarin red dye binds with the calcium phosphate compounds of the mineralized extracellular matrix of cells and helps to stain the monolayer red. The dye can be eluted and quantified using a protocol followed previously [78]. From Figures 4.26 and 4.27, it is seen that all the composites showed better mineralization which is a direct indication of the differentiated cells, as late stage marker, when compared with hydroxyapatite which served as the control. HAP-K100 and HAP-K125 showed better *in vitro* biomineralization, of which the organic to inorganic content matched with that of the natural bone. The role of bone-mimetic materials to help in better osteogenic differentiation is well known [109] which enhances the osteogenic differentiation potential, and it is seen that keratin-hydroxyapatite based organo-apatites also serve as bone-mimetic materials.



(Figure – 4.26: Alizarin stained cells in presence of A) HAP, B) HAP-K50, C) HAP-K75, D) HAP-K100, E) HAP-K125 and F) HAP-K150)

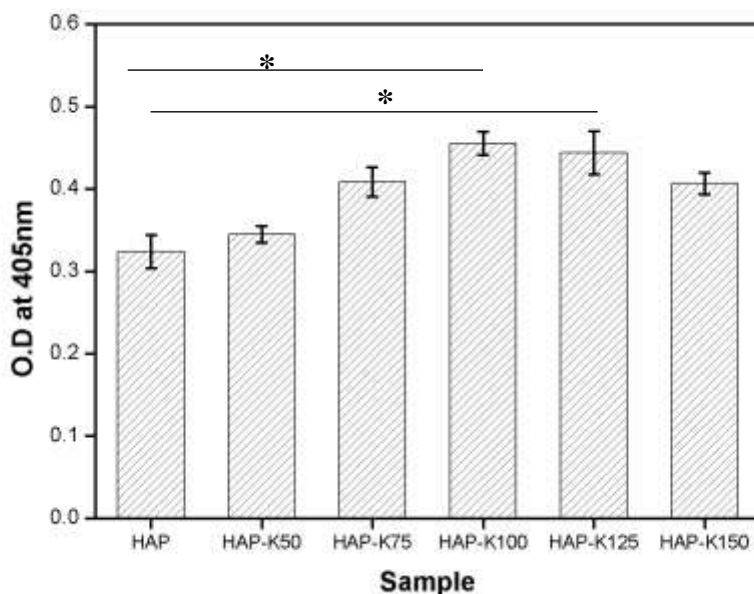


Figure – 4.27: Alizarin red assay in presence of hydroxyapatite and organo-apatites; each point represents the mean \pm SD ($n=3$), * represents significant difference between the population mean at $p < 0.05$

4.3.3.2 Alkaline Phosphatase Assay:

Alkaline phosphatase (ALP) is a key early osteogenic marker which is expressed in osteogenic cells, as a result the ALP cleaves the phosphate esters to liberate phosphate which is essential for bone mineralization in early stage of differentiation [77, 110]. The ALP is expressed between day 7 to 14 and hence its expression is studied to analyze the osteogenic differentiation potential of the ADSCs in presence of the organo-apatite composites. From Figure-4.28 it is seen that at Day-14 there is a surge of ALP expression indicating that the ALP is an early differentiation marker, and all the composites showed better ALP expression than the HAP as control. HAP-K100 and HAP-K125 exhibited the maximum ALP expression, of which the organic to inorganic ratio is closely matching with that of the bone. It is seen that ALP is very important for bone-mineralization and the composites HAP-K100 showed higher ALP expression and it is seen in alizarin red assay, cells seeded with HAP-K100 exhibited higher biomineralization which is due to the reason of higher expression of ALP induced by HAP-K100 composite.

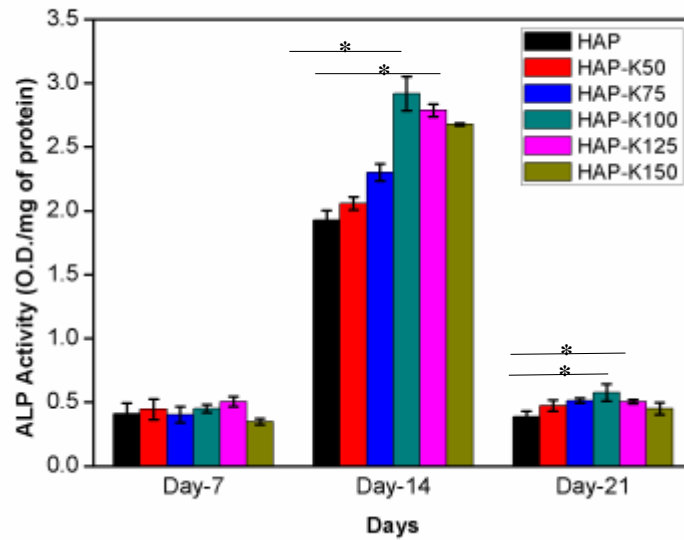


Figure – 4.28: Alkaline phosphatase assay in presence of hydroxyapatite and organo-apatites; each point represents the mean \pm SD ($n = 3$), * represents significant difference between the population mean at $p < 0.05$

4.3.3.3 Osteocalcin and Run-x2 Expression:

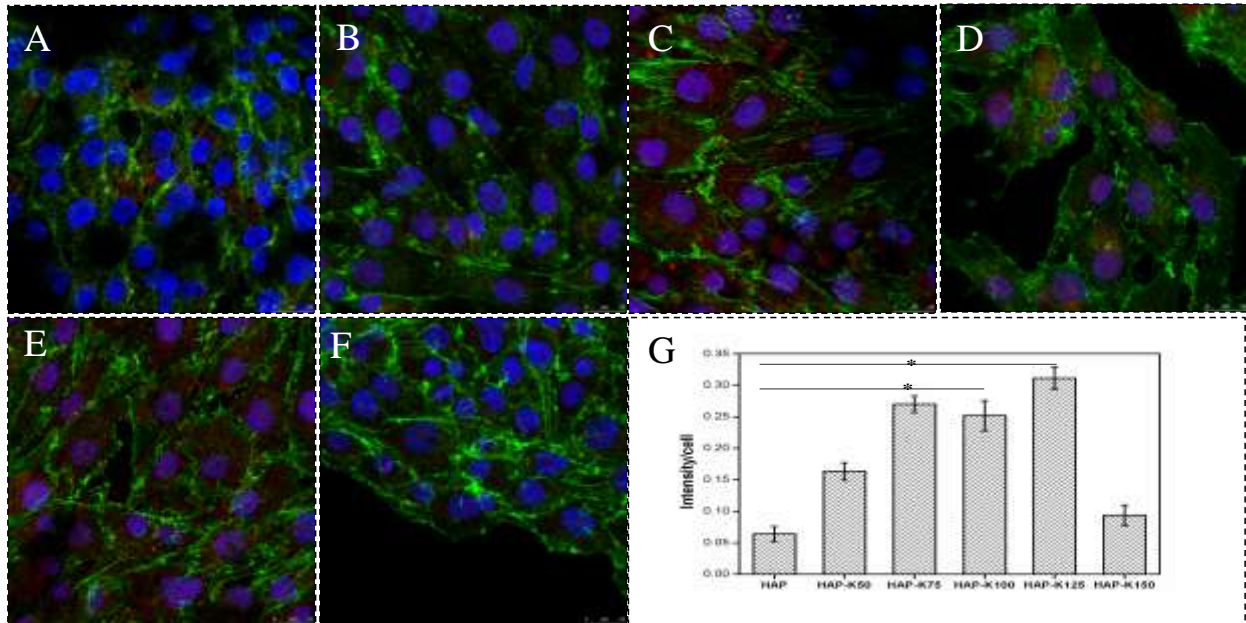


Figure – 4.29: Osteocalcin expression after 21 days in presence of A) HAP, B) HAP-K50, C) HAP-K75, D) HAP-K100, E) HAP-K125, F) HAP-K150 and intensity/cell plot for osteocalcin expression, where each point represents the mean \pm SD ($n = 3$), * represents significant difference between the population mean at $p < 0.05$

Expression of osteocalcin which is an important protein responsible for bonemineralization is expressed in terminally differentiated osteocytes, which is regulated by Cbfa/Runx-2 [111]. Osteocalcin which is a late osteoblast marker [112] which helps to regulate osteoclast activity has a binding affinity to calcium and thus helping in bone bio-mineralization process. Therefore checking the level of expression of osteocalcin helps us to understand the osteogenic differentiation potential of ADSCs in presence of the organo-apatites. It is seen from the Figure-4.29, HAP-K125 shows high expression of osteocalcin which is similar to that of the bone's organic to inorganic matrix content. Hence it is proved that the keratin based organo-apatites which are closely matching with the bone's matrix is helpful in osteogenic differentiation.

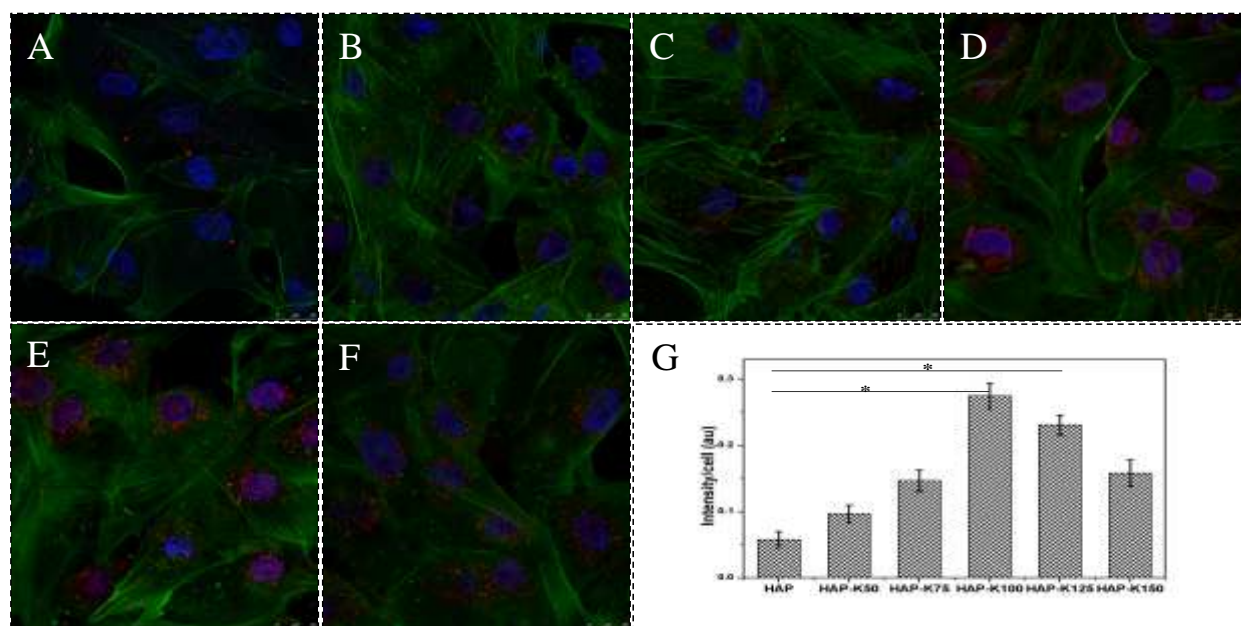


Figure – 4.30: Runx2 expression after 7 days in presence of A) HAP, B) HAP-K50, C) HAP-K75, D) HAP-K100, E) HAP-K125, F) HAP-K150 and intensity/cell plot for Runx2 expression, where each point represents the mean \pm SD ($n=3$), * represents significant difference between the population mean at $p < 0.05$

From Figure-4.30 it is seen that the expression of a key transcription factor, Runx2 (Runt-related transcription factor-2) which holds the switch for the osteogenic differentiation in adult stem cells by helping downstream regulation of ALP, osteocalcin and several other osteogenic markers. The runx2 is localized within and surrounding the nucleus and is found to be increasing in all the composites with HAP-K100 and HAP-K125 being the highest. It is known that keratin consists of binding domain for the α -4 and α -5 integrin receptors enhancing its cell adhesion

properties.[17, 18] The binding of ADSCs to these α -4 and α -5 integrin helps in adhesion (as inferred from cytoskeletal architecture assessment), and differentiation [109]. The HAP-K100 and HAP-K125 which has a close bone-mimetic property due to its organic to inorganic ratio aspect helps to regulate the α -4 and α -5 integrin mediated pathway for activation of runx2 expression. It was observed that the bone biomineralization was increased by 65% due to the activation of osteoblast integrin adhesion mediated downstream pathways which involved runx2 mediated activation of osteogenic markers.[113, 114] The HAP-K100 and HAP-K125 act as bone mimetic materials which help in mimicking the micro-environment and thus activate the Ras/ERK pathway which activates the transcription factor Runx2, which in turn helps to activate key osteogenic differentiation markers like ALP, BSP (bone sialoprotein) and osteocalcin. [58] Thus keratin based organo-apatites (HAP-K100 and HAP-K125) which mimic the bone's organic to inorganic content were found to be more osteo-conductive and bio-compatible and can be successfully implied for bone tissue engineering application.

5. CONCLUSION

In recent years much interest is gained in the area of curing critical sized bone defects which occur during primary tumor segmentectomy, trauma or accidental injury to the bone. Though the bone has innate self-healing capability, the mending of critical size defects arising due to the mentioned causes puts up a real challenge. For treating such critical sized defects, engineered materials which mimic the bone's physical and chemical properties, such as organoapatites, self-assembled apatite on amphiphiles and collagen-hydroxyapatite nanocomposites are increasingly used. The hard α -keratin found in hair is an ideal candidate for synthesis of bone-mimetic organo-apatite, since it being a majorly helical protein suitable for the nucleation of the apatite crystals, just like the collagen type-I present in the bone. Keratin possesses key amino acid motifs such as RGD (arginine-glycine-aspartate) and LDV (leucine-aspartate-valine) and EDS (glutamate-aspartate-serine) to which $\alpha 5$, α -4 integrin receptor family binds and hence enhancing its cell adhesion properties.

The first part of the study was to determine a suitable method of extraction of keratin from human hair. There has been no study carried out till now on the effect of extraction procedure on the stability of keratin from human hair. A comparative study between two well-known protocols namely Shindai and Sodium sulfide methods was carried out for the extraction of keratin from human hair. It was found that the sodium sulfide method was relatively a better method for extraction of keratin because of its yield (12.19 ± 0.422 mg/ml), ease of extraction, and stability of the extracted protein whose zeta potential was found to be -32.5 ± 4.36 mV. It was found that the extracted keratin by sodium sulfide method comprised of 29% α -helix, 25% β -sheet, 27% β -sheet and 17% disordered structures. Thus the sodium sulfide method helped to conserve the structural integrity of the extracted keratin, whose secondary structures were mostly retained which was inferred through the FTIR, XRD and CD analysis.

The second part of the study was to use the keratin extracted by sodium sulfide method for the synthesis of organo-apatites. A total of 5 different keratin based organo-apatites namely HAP-K50, HAP-K75, HAP-K100, HAP-K125 and HAP-K150 were synthesized with different concentrations of keratin through co-precipitation method. The phase analysis of the synthesized organo-apatites was done using XRD which revealed the keratin in the composites decreased the crystallinity and size of the apatite formed. The functional analysis done using FTIR and CD and

the morphological observation using FESEM showed heterogenous nucleation and growth of rod shaped 20-30nm apatite crystals along the keratin fibril. The thermal analysis helped to determine that the composites HAP-K100 and HAP-K125 had an organic to in-organic content similar to that of the bone. The HAP-K100 and HAP-K125 were found to be more bio-active than the other composites with a moderate bio-degradability and a young's moduli of 2.02 ± 0.07 and 1.21 ± 0.06 MPa respectively which is relevant for application as bone fillers. The *in vitro* cell study carried out revealed that HAP-K100 and HAP-K125 showed superior cell supportive property achieving better cell spreadability, cell proliferation and metabolic activity. Furthermore enhanced osteogenic differentiation potential of these composites assessed through alizarin red assay, ALP assay and Runx2 and osteocalcin expression demonstrated that the composites HAP-K100 and HAP-K125 can be used as bone-mimetic biomaterials for bone tissue engineering applications.

REFERENCES

1. Porter, J.R., T.T. Ruckh, and K.C. Popat, *Bone tissue engineering: a review in bone biomimetics and drug delivery strategies*. Biotechnology Progress, 2009. **25**(6): p. 1539-1560.
2. Palmer, L.C., et al., *Biomimetic systems for hydroxyapatite mineralization inspired by bone and enamel*. Chemical Reviews, 2008. **108**(11): p. 4754-4783.
3. Kikuchi, M., et al., *Biomimetic synthesis of bone-like nanocomposites using the self-organization mechanism of hydroxyapatite and collagen*. Composites Science and Technology, 2004. **64**(6): p. 819-825.
4. Reichl, S., *Films based on human hair keratin as substrates for cell culture and tissue engineering*. Biomaterials, 2009. **30**(36): p. 6854-6866.
5. Cui, F.-Z., Y. Li, and J. Ge, *Self-assembly of mineralized collagen composites*. Materials Science and Engineering: R: Reports, 2007. **57**(1): p. 1-27.
6. Liao, S., et al., *Hierarchically biomimetic bone scaffold materials: nano-HA/collagen/PLA composite*. Journal of Biomedical Materials Research Part B: Applied Biomaterials, 2004. **69**(2): p. 158-165.
7. Weiner, S. and H.D. Wagner, *The material bone: structure-mechanical function relations*. Annual Review of Materials Science, 1998. **28**(1): p. 271-298.
8. Stupp, S.I. and G.W. Ciegler, *Organoapatites: materials for artificial bone. I. Synthesis and microstructure*. Journal of biomedical materials research, 1992. **26**(2): p. 169-183.
9. Yamauchi, K., et al., *Enhanced cell adhesion on RGDS-carrying keratin film*. Materials Science and Engineering: C, 2003. **23**(4): p. 467-472.
10. Porter, R.M., *The new keratin nomenclature*. J Invest Dermatol, 2006. **126**(11): p. 2366-8.
11. Hill, P., H. Brantley, and M. Van Dyke, *Some properties of keratin biomaterials: kerateines*. Biomaterials, 2010. **31**(4): p. 585-593.
12. Yu, J., et al., *Human Hair Keratins*. J Investig Dermatol, 1993. **101**(s1): p. 56S-59S.
13. Shimomura, Y. and M. Ito. *Human hair keratin-associated proteins*. in *The journal of investigative dermatology. Symposium proceedings/the Society for Investigative Dermatology, Inc.[and] European Society for Dermatological Research*. 2005.

14. Nakamura, A., et al., *A rapid extraction procedure of human hair proteins and identification of phosphorylated species*. Biological and Pharmaceutical Bulletin, 2002. **25**(5): p. 569-572.
15. de Guzman, R.C., et al., *Mechanical and biological properties of keratose biomaterials*. Biomaterials, 2011. **32**(32): p. 8205-8217.
16. Verma, V., et al., *Preparation of scaffolds from human hair proteins for tissue-engineering applications*. Biomedical Materials, 2008. **3**(2): p. 025007.
17. Rouse, J.G. and M.E. Van Dyke, *A review of keratin-based biomaterials for biomedical applications*. Materials, 2010. **3**(2): p. 999-1014.
18. Humphries, J.D., A. Byron, and M.J. Humphries, *Integrin ligands at a glance*. Journal of cell science, 2006. **119**(19): p. 3901-3903.
19. Yamauchi, K., M. Maniwa, and T. Mori, *Cultivation of fibroblast cells on keratin-coated substrata*. Journal of Biomaterials Science, Polymer Edition, 1998. **9**(3): p. 259-270.
20. Wang, S., et al., *Human keratin hydrogels support fibroblast attachment and proliferation in vitro*. Cell and tissue research, 2012. **347**(3): p. 795-802.
21. Blanchard, C.R., S.F. Timmons, and R.A. Smith, *Keratin-based hydrogel for biomedical applications and method of production*, 1999, Google Patents.
22. Van Dyke, M.E., et al., *Soluble keratin peptide*, 2001, Google Patents.
23. Tseng, F.-C.J., *Biofibre production from chicken feather*, 2011, University of Waikato.
24. Alexander, P. and C. Earland, *Structure of Wool Fibres: Isolation of an alpha-and beta-Protein in Wool*. Nature, 1950. **166**: p. 396-397.
25. Haylett, T., et al., *A Physicochemical Study of the High-Sulfur Proteins from Oxidized Wool*. Textile Research Journal, 1963. **33**(8): p. 639-649.
26. O'donnell, I. and E. Thompson, *Studies on Oxidised Wool. II. Extraction of Soluble Proteins From Wool Oxidized With Performic Acid*. Australian Journal of Biological Sciences, 1959. **12**(3): p. 294-302.
27. Burnett, L. and S.A. Boyd, *Methods for extracting keratin proteins*, 2012, Google Patents.
28. Robbins, C.R., *Chemical and physical behavior of human hair*. Vol. 4. 2002: Springer.
29. Saul, J.M., et al., *Keratin hydrogels support the sustained release of bioactive ciprofloxacin*. Journal of biomedical materials research Part A, 2011. **98**(4): p. 544-553.

30. Corfield, M., A. Robson, and B. Skinner, *The amino acid compositions of three fractions from oxidized wool*. Biochemical Journal, 1958. **68**(2): p. 348.
31. Poole, A.J., R.E. Lyons, and J.S. Church, *Dissolving feather keratin using sodium sulfide for bio-polymer applications*. Journal of Polymers and the Environment, 2011. **19**(4): p. 995-1004.
32. Hill, P.S., H. Brantley, and M. Van Dyke, *Properties and biocompatibility of keratin biomaterials derived from human hair part i: kerateine. regeneration of peripheral nerves using neuroinductive biomaterial scaffolds*, 2009: p. 80.
33. Lau, S., A. Taneja, and R. Hodges, *Synthesis of a model protein of defined secondary and quaternary structure. Effect of chain length on the stabilization and formation of two-stranded alpha-helical coiled-coils*. Journal of Biological Chemistry, 1984. **259**(21): p. 13253-13261.
34. Dunbar, J., et al., *The effect of denaturants on protein structure*. Protein science, 1997. **6**(8): p. 1727-1733.
35. Clark, E.D.B., *Protein refolding for industrial processes*. Current Opinion in Biotechnology, 2001. **12**(2): p. 202-207.
36. Middelberg, A.P., *Preparative protein refolding*. TRENDS in Biotechnology, 2002. **20**(10): p. 437-443.
37. Steinert, P.M., *The extraction and characterization of bovine epidermal alpha-keratin*. Biochem. j, 1975. **149**: p. 39-48.
38. Miyamoto, Y., et al., *Basic properties of calcium phosphate cement containing atelocollagen in its liquid or powder phases*. Biomaterials, 1998. **19**(7-9): p. 707-715.
39. Martins, A., V. Conceição, and G. Goissis, *Nonstoichiometric Hydroxyapatite-Anionic Collagen Composite as Support for the Double Sustained Release of Gentamicin and Norfloxacin/Ciprofloxacin*. Artificial organs, 2000. **24**(3): p. 224-230.
40. Kikuchi, M., et al., *Self-organization mechanism in a bone-like hydroxyapatite/collagen nanocomposite synthesized in vitro and its biological reaction in vivo*. Biomaterials, 2001. **22**(13): p. 1705-1711.
41. Sinha, A., et al., *Synthesis of nanosized and microporous precipitated hydroxyapatite in synthetic polymers and biopolymers*. Journal of the American Ceramic Society, 2003. **86**(2): p. 357-359.

42. Nayar, S. and A. Sinha, *Protein induced morphosynthesis of calcium carbonate*. Journal of materials science letters, 2003. **22**(3): p. 167-170.
43. Sinha, A., et al., *Morphosynthesis of calcium carbonate in poly (vinylalcohol)*. Journal of Materials Synthesis and Processing, 2002. **10**(3): p. 149-153.
44. Verde-Carvalho, G., A. Guarino, and G. González, *Mineralization of hydroxyapatite over collagen type I*. European Cells and Materials, 2004. **7**(2): p. 58-59.
45. Yamauchi, K., et al., *Preparation of collagen/calcium phosphate multilayer sheet using enzymatic mineralization*. Biomaterials, 2004. **25**(24): p. 5481-5489.
46. Tampieri, A., et al., *HA/alginate hybrid composites prepared through bio-inspired nucleation*. Acta biomaterialia, 2005. **1**(3): p. 343-351.
47. Takeuchi, A., et al., *Heterogeneous nucleation of hydroxyapatite on protein: structural effect of silk sericin*. Journal of The Royal Society Interface, 2005. **2**(4): p. 373-378.
48. Wahl, D. and J. Czernuszka, *Collagen-hydroxyapatite composites for hard tissue repair*. Eur Cell Mater, 2006. **11**: p. 43-56.
49. Zhai, Y. and F. Cui, *Recombinant human-like collagen directed growth of hydroxyapatite nanocrystals*. Journal of crystal growth, 2006. **291**(1): p. 202-206.
50. Zhang, F., et al., *Study of growth of calcium carbonate crystals on chitosan film*. Materials & design, 2006. **27**(5): p. 422-426.
51. Liao, S., et al., *Self-assembly of nano-hydroxyapatite on multi-walled carbon nanotubes*. Acta biomaterialia, 2007. **3**(5): p. 669-675.
52. Wang, J., et al., *Collagen/silk fibroin bi-template induced biomimetic bone-like substitutes*. Journal of biomedical materials research Part A, 2011. **99**(3): p. 327-334.
53. Kim, G.-M., G. MICHLER, and P. PÖTSCHKE, *Fabrication of bio-nanocomposite nanofibers mimicking the mineralized hard tissues via electrospinning process*2010: INTECH Open Access Publisher.
54. Zhao, H., et al., *In vitro biomimetic construction of hydroxyapatite–porcine acellular dermal matrix composite scaffold for MC3T3-E1 preosteoblast culture*. Tissue Engineering Part A, 2010. **17**(5-6): p. 765-776.
55. Li, J.-S., et al., *Strategy to introduce an hydroxyapatite–keratin nanocomposite into a fibrous membrane for bone tissue engineering*. Journal of Materials Chemistry B, 2013. **1**(4): p. 432-437.

56. Kochi, A., et al., *Preparation of injectable hydroxyapatite/collagen nanocomposite artificial bone*. Key Engineering Materials, 2012. **493**: p. 689-692.
57. Declercq, H., et al., *Isolation, proliferation and differentiation of osteoblastic cells to study cell/biomaterial interactions: comparison of different isolation techniques and source*. Biomaterials, 2004. **25**(5): p. 757-768.
58. Langenbach, F. and J. Handschel, *Effects of dexamethasone, ascorbic acid and β -glycerophosphate on the osteogenic differentiation of stem cells in vitro*. Stem Cell Res Ther, 2013. **4**(5): p. 117.
59. Coelho, M. and M. Fernandes, *Human bone cell cultures in biocompatibility testing. Part II: effect of ascorbic acid, β -glycerophosphate and dexamethasone on osteoblastic differentiation*. Biomaterials, 2000. **21**(11): p. 1095-1102.
60. Jaiswal, N., et al., *Osteogenic differentiation of purified, culture-expanded human mesenchymal stem cells in vitro*. Journal of cellular biochemistry, 1997. **64**(2): p. 295-312.
61. Tenenbaum, H.C. and J.N. Heersche, *Dexamethasone stimulates osteogenesis in chick periosteum in vitro*. Endocrinology, 1985. **117**(5): p. 2211-2217.
62. Song, I.H., A.I. Caplan, and J.E. Dennis, *Dexamethasone inhibition of confluence-induced apoptosis in human mesenchymal stem cells*. Journal of Orthopaedic Research, 2009. **27**(2): p. 216-221.
63. Phillips, J.E., et al., *Glucocorticoid-induced osteogenesis is negatively regulated by Runx2/Cbfa1 serine phosphorylation*. Journal of cell science, 2006. **119**(3): p. 581-591.
64. Park, J.-B., *The effects of dexamethasone, ascorbic acid, and β -glycerophosphate on osteoblastic differentiation by regulating estrogen receptor and osteopontin expression*. Journal of Surgical Research, 2012. **173**(1): p. 99-104.
65. Choi, K.-M., et al., *Effect of ascorbic acid on bone marrow-derived mesenchymal stem cell proliferation and differentiation*. Journal of bioscience and bioengineering, 2008. **105**(6): p. 586-594.
66. Locke, M., J. Windsor, and P. Dunbar, *Human adipose-derived stem cells: isolation, characterization and applications in surgery*. ANZ journal of surgery, 2009. **79**(4): p. 235-244.

67. Vater, C., P. Kasten, and M. Stiehler, *Culture media for the differentiation of mesenchymal stromal cells*. Acta biomaterialia, 2011. **7**(2): p. 463-477.
68. Tachibana, A., et al., *Rapid fabrication of keratin–hydroxyapatite hybrid sponges toward osteoblast cultivation and differentiation*. Biomaterials, 2005. **26**(3): p. 297-302.
69. Li, J., et al., *Preparation and biodegradation of electrospun PLLA/keratin nonwoven fibrous membrane*. Polymer Degradation and Stability, 2009. **94**(10): p. 1800-1807.
70. Dias, G.J., et al., *Keratin–hydroxyapatite composites: Biocompatibility, osseointegration, and physical properties in an ovine model*. Journal of biomedical materials research Part A, 2010. **95**(4): p. 1084-1095.
71. Bradford, M.M., *A rapid and sensitive method for the quantitation of microgram quantities of protein utilizing the principle of protein-dye binding*. Analytical biochemistry, 1976. **72**(1): p. 248-254.
72. Sambrook, J., E. Fritsch, and T. Maniatis, *SDS-polyacrylamide gel electrophoresis of proteins*. Molecular cloning: a laboratory manual, 1989. **3**: p. 18.47-18.59.
73. Tank, K.P., et al., *Cobalt-doped nanohydroxyapatite: synthesis, characterization, antimicrobial and hemolytic studies*. Journal of nanoparticle research, 2013. **15**(5): p. 1-11.
74. Tas, A.C., *Synthesis of biomimetic Ca-hydroxyapatite powders at 37 C in synthetic body fluids*. Biomaterials, 2000. **21**(14): p. 1429-1438.
75. Grunenwald, A., et al., *Revisiting carbonate quantification in apatite (bio) minerals: a validated FTIR methodology*. Journal of Archaeological Science, 2014. **49**: p. 134-141.
76. Thein-Han, W. and R. Misra, *Biomimetic chitosan–nanohydroxyapatite composite scaffolds for bone tissue engineering*. Acta biomaterialia, 2009. **5**(4): p. 1182-1197.
77. Marom, R., et al., *Characterization of adhesion and differentiation markers of osteogenic marrow stromal cells*. Journal of cellular physiology, 2005. **202**(1): p. 41-48.
78. Gregory, C.A., et al., *An Alizarin red-based assay of mineralization by adherent cells in culture: comparison with cetylpyridinium chloride extraction*. Analytical Biochemistry, 2004. **329**(1): p. 77-84.
79. Faulstich, H., H. Trischmann, and D. Mayer, *Preparation of tetramethylrhodaminyl-phalloidin and uptake of the toxin into short-term cultured hepatocytes by endocytosis*. Experimental cell research, 1983. **144**(1): p. 73-82.

80. Li, J., et al., *Synthesis and characterization of wool keratin/hydroxyapatite nanocomposite*. Journal of Biomedical Materials Research Part B: Applied Biomaterials, 2012. **100**(4): p. 896-902.
81. Vasconcelos, A., G. Freddi, and A. Cavaco-Paulo, *Biodegradable materials based on silk fibroin and keratin*. Biomacromolecules, 2008. **9**(4): p. 1299-1305.
82. Cardamone, J.M., *Investigating the microstructure of keratin extracted from wool: Peptide sequence (MALDI-TOF/TOF) and protein conformation (FTIR)*. Journal of molecular structure, 2010. **969**(1): p. 97-105.
83. de Aragão, B.J. and Y. Messaddeq, *Peak separation by derivative spectroscopy applied to ftir analysis of hydrolized silica*. Journal of the Brazilian Chemical Society, 2008. **19**(8): p. 1582-1594.
84. Kreplak, L., et al., *New aspects of the alpha-helix to beta-sheet transition in stretched hard alpha-keratin fibers*. Biophys J, 2004. **87**(1): p. 640-7.
85. Steinert, P.M., W.W. Idler, and S.B. Zimmerman, *Self-assembly of bovine epidermal keratin filaments < i > in vitro < /i >*. Journal of molecular biology, 1976. **108**(3): p. 547-567.
86. Er Rafik, M., J. Doucet, and F. Briki, *The Intermediate Filament Architecture as Determined by X-Ray Diffraction Modeling of Hard α -Keratin*. Biophysical Journal, 2004. **86**(6): p. 3893-3904.
87. Li, S. and X.-H. Yang, *Fabrication and Characterization of Electrospun Wool Keratin/Poly (vinyl alcohol) Blend Nanofibers*. Advances in Materials Science and Engineering, 2014. **2014**.
88. Idris, A., et al., *Dissolution of feather keratin in ionic liquids*. Green Chemistry, 2013. **15**(2): p. 525-534.
89. Tachibana, A., et al., *Fabrication of wool keratin sponge scaffolds for long-term cell cultivation*. Journal of Biotechnology, 2002. **93**(2): p. 165-170.
90. Kakkar, P., B. Madhan, and G. Shanmugam, *Extraction and characterization of keratin from bovine hoof: A potential material for biomedical applications*. SpringerPlus, 2014. **3**(1): p. 596.

91. Koutsopoulos, S., *Synthesis and characterization of hydroxyapatite crystals: a review study on the analytical methods*. Journal of biomedical materials research, 2002. **62**(4): p. 600-612.
92. Wijesinghe, W., et al., *Facile synthesis of both needle-like and spherical hydroxyapatite nanoparticles: Effect of synthetic temperature and calcination on morphology, crystallite size and crystallinity*. Materials Science and Engineering: C, 2014. **42**: p. 83-90.
93. Capriotti, L.A., T.P. Beebe, and J.P. Schneider, *Hydroxyapatite surface-induced peptide folding*. Journal of the American Chemical Society, 2007. **129**(16): p. 5281-5287.
94. Litvinov, R.I., et al., *The α -helix to β -sheet transition in stretched and compressed hydrated fibrin clots*. Biophysical journal, 2012. **103**(5): p. 1020-1027.
95. Kreplak, L., et al., *New aspects of the α -helix to β -sheet transition in stretched hard α -keratin fibers*. Biophysical journal, 2004. **87**(1): p. 640-647.
96. Mir, M., et al., *XRD, AFM, IR and TGA study of nanostructured hydroxyapatite*. Materials Research, 2012. **15**(4): p. 622-627.
97. Singh, A., *Hydroxyapatite, a biomaterial: Its chemical synthesis, characterization and study of biocompatibility prepared from shell of garden snail, Helix aspersa*. Bulletin of Materials Science, 2012. **35**(6): p. 1031-1038.
98. Olszta, M.J., et al., *Bone structure and formation: a new perspective*. Materials Science and Engineering: R: Reports, 2007. **58**(3): p. 77-116.
99. Kane, R.J., et al., *Hydroxyapatite reinforced collagen scaffolds with improved architecture and mechanical properties*. Acta biomaterialia, 2015. **17**: p. 16-25.
100. Mason, P., *Density and structure of alpha-keratin*. 1963.
101. Lee, K., et al., *Effect of surface properties on the antithrombogenicity of silk fibroin/S-carboxymethyl kerateine blend films*. Journal of Biomaterials Science, Polymer Edition, 1998. **9**(9): p. 905-914.
102. Aboushwareb, T., et al., *A keratin biomaterial gel hemostat derived from human hair: evaluation in a rabbit model of lethal liver injury*. Journal of Biomedical Materials Research Part B: Applied Biomaterials, 2009. **90**(1): p. 45-54.
103. Kokubo, T. and H. Takadama, *How useful is SBF in predicting in vivo bone bioactivity?* Biomaterials, 2006. **27**(15): p. 2907-2915.

104. Spitzer, R.S., et al., *Matrix engineering for osteogenic differentiation of rabbit periosteal cells using α -tricalcium phosphate particles in a three-dimensional fibrin culture*. Journal of biomedical materials research, 2002. **59**(4): p. 690-696.
105. Rodrigues, C., et al., *Characterization of a bovine collagen–hydroxyapatite composite scaffold for bone tissue engineering*. Biomaterials, 2003. **24**(27): p. 4987-4997.
106. Burg, K.J., S. Porter, and J.F. Kellam, *Biomaterial developments for bone tissue engineering*. Biomaterials, 2000. **21**(23): p. 2347-2359.
107. Kim, H.J., et al., *Bone tissue engineering with premineralized silk scaffolds*. Bone, 2008. **42**(6): p. 1226-1234.
108. Jang, J.-H., et al., *Enhanced fibronectin-mediated cell adhesion of human osteoblast by fibroblast growth factor, FGF-2*. Biotechnology letters, 2002. **24**(20): p. 1659-1663.
109. Shekaran, A. and A.J. García, *Extracellular matrix-mimetic adhesive biomaterials for bone repair*. Journal of biomedical materials research Part A, 2011. **96**(1): p. 261-272.
110. Granéli, C., et al., *Novel markers of osteogenic and adipogenic differentiation of human bone marrow stromal cells identified using a quantitative proteomics approach*. Stem cell research, 2014. **12**(1): p. 153-165.
111. Birmingham, E., G. Niebur, and P. McHugh, *Osteogenic differentiation of mesenchymal stem cells is regulated by osteocyte and osteoblast cells in a simplified bone niche*. 2012.
112. Nakashima, K., et al., *The novel zinc finger-containing transcription factor osterix is required for osteoblast differentiation and bone formation*. Cell, 2002. **108**(1): p. 17-29.
113. Salter, D., J. Robb, and M. Wright, *Electrophysiological responses of human bone cells to mechanical stimulation: evidence for specific integrin function in mechanotransduction*. Journal of Bone and Mineral Research, 1997. **12**(7): p. 1133-1141.
114. Schneider, G., R. Zaharias, and C. Stanford, *Osteoblast integrin adhesion and signaling regulate mineralization*. Journal of dental research, 2001. **80**(6): p. 1540-1544.